**MMS**

**S Sage**

# Computational integration and experimental validation of a two-length scale model for accurate prediction of steels' plastic behavior during phase transformation

**Koffi Enakoutsa**
*Department of Mathematics, University of California, Los Angeles, Los Angeles, CA, USA*

**Yanni L Bills**
*Department of Mathematics, University of California, Los Angeles, Los Angeles, CA, USA*

## Abstract

Transformation plasticity, essential during solid–solid phase transitions, significantly impacts industrial processes like welding and quenching. Accurately simulating these procedures necessitates understanding thermal, metallurgical, and mechanical effects. Leblond et al.'s model offers a foundation, but refinement for mixed isotropic/kinematic hardening is crucial. We enhance this model by introducing characteristic length scales through nonlocal variables, illuminating plastic deformation mechanisms in both phases. Our work includes numerical implementation within a finite element analysis framework and practical applications to phase transformation scenarios involving A.508 cl. 3 and A533 low-alloy steels. Results affirm model robustness and efficiency in predicting phase transformation phenomena, benefiting industrial applications.

## 1. Introduction

Transformation plasticity was coined to describe the intriguing plastic behavior exhibited by metals and alloys during solid–solid phase transitions. These transformations typically manifest during the cooling phase of thermo-mechanical processes such as welding [1] and quenching [2]. In these thermo-mechanical processes, which are prevalent in various industries, three key physical phenomena interact: thermal, metallurgical, and mechanical. To enable accurate numerical simulations of welding and quenching processes, it is essential to incorporate these thermal, metallurgical, and mechanical effects into computational codes. This ensures the development of robust numerical tools for predicting the behavior of industrial components undergoing these thermo-mechanical procedures. During these processes, thermal and mechanical actions cause phase transformations, leading to transformation deformations.

**Corresponding author:**
Koffi Enakoutsa, Department of Mathematics, University of California, Los Angeles, Los Angeles, CA 90095-1555, USA.
Email: koffi@math.ucla.edu

Over the years, numerous studies, including those conducted by Fukumoto et al. [3], Miyao et al. [4], and Taleb and Sidoroff [5], among others, have extensively highlighted the substantial impact of transformation plasticity on residual stresses and distortions resulting from such treatments. This significant influence serves as a pivotal motivation driving the continuous development of robust transformation plasticity models. These models are essential for their integration into finite element programs, enabling engineers and researchers to make precise predictions of residual stresses and distortions induced by complex thermo-mechanical processes, thereby enhancing the efficacy and reliability of industrial applications.

The plastic behaviors of steels during phase transformation can be divided into two groups:

- Classical plasticity, i.e., the response of the material (mixture of two phases) to variations of applied stress or temperature.
- Transformation plasticity, i.e., the response of the material to variations of the phase proportions.

It is commonly accepted that transformation plasticity is attributed to two primary mechanisms, one being diffusive [6] and the other being displacive [7].

- In the seminal work by Greenwood and Johnson [6], transformation plasticity is explained as originating from the standard dislocation-induced plasticity occurring at the microscopic level within the weaker mother phase. This phase, predominant at elevated temperatures and typically characterized by a considerably lower yield stress, experiences microscopic plastic deformation due to the difference in specific volume between the coexisting phases during transformation, constituting the volumetric portion of the transformation strain. As a result, significant internal stresses are generated, effectively initiating plasticity within the weaker phase. Importantly, this effect persists even in the absence of external stress. However, the presence of external stress capitalizes on the inherent "transformation-induced weakness" of the material, thereby facilitating plastic deformation.
- Contrary to prevailing orthodoxies, Magee and Paxton's [7] seminal work in 1966 offers a paradigm-shifting interpretation of transformation plasticity. Magee posits that this phenomenon diverges markedly from conventional plasticity mechanisms, emanating instead from the deviatoric component of the transformation strain localized within the transitioning regions. While Magee concedes the potential inadequacy of the term "transformation plasticity" to fully encapsulate this interpretation, given the inherently pseudo-elastic and reversible nature of the transformation strain driving the effect, he asserts its continued usage as a classical term in the field. From Magee's nuanced perspective, in the absence of external stress, the deviatoric fraction of the transformation strain within the material exhibits stochastic directional fluctuations, effectively averaging to nullity. However, under the influence of nonzero external stress, this deviatoric component aligns, engendering discernible macroscopic strain. This refined understanding of transformation plasticity not only challenges entrenched orthodoxies but also offers a profound glimpse into the intricate mechanics underpinning this phenomenon.

The principle of Greenwood and Johnson [6] transformation plasticity mechanism lies in the plastic accommodation of the austenite phase (the softer phase) during the phase transformation (this idea originates from the pioneering work of De Jong and Rathenau [8]). During cooling, the austenitic $\gamma$ phase gives rise to a ferritic, bainitic, or martensitic $\alpha$ phase, which has a greater specific volume than its parent phase, see Bhadeshia [9, 10]. When both phases coexist, the volume difference between them generates a field of heterogeneous deformation, resulting in internal stresses and macroscopic plastic flow, even if the macroscopic applied stress is below the yield strength of both phases or even zero. The first micro-mechanical model of this mechanism, established by Leblond et al. [11, 12], considers a representative spherical volume element of an expanding $\alpha$ phase core, surrounded by a concentric spherical shell of $\gamma$ phase. When considering low macroscopic stresses, this approach leads to an expression for the rate of transformation plastic deformation that is linearly dependent on the deviatoric part of stresses.

The popularity of this model can likely be attributed to its simplicity and practicality. One of its key strengths lies in the formulation of the transformation plastic strain rate, which solely relies on standard mechanical parameters of the two phases: the yield stress of the weaker phase and the volumetric transformation strain. Remarkably, it does not require any additional "ad hoc" parameters that need to be determined experimentally. This feature is particularly advantageous for applications in numerical simulations of thermo-mechanical treatments. In many cases, experimental data related to transformation plasticity for the specific material under consideration are unavailable. Therefore, the model's reliance on readily accessible mechanical parameters

renders it highly versatile and applicable across a wide range of scenarios without the need for extensive experimental calibration.

To delve deeper into this subject, it is imperative to recognize that the behavior of metals during phase transformations is a critical aspect of materials engineering. Phase transformations can dramatically influence a material's properties, such as strength, ductility, and thermal conductivity, making them central to the design and performance of various engineering structures and components. The work-hardening isotropic-kinematic model is particularly significant in this context because it offers a versatile and robust tool for characterizing and predicting the mechanical response of materials as they undergo phase transformations. It encompasses both isotropic hardening, which accounts for the evolution of the yield stress with deformation, and kinematic hardening, which considers the evolution of the material's anisotropy.

Phase transformation in steels is a complex phenomenon influenced by various factors operating at different length scales. Traditional models often neglect the intricate interactions between microstructural features, leading to inaccuracies in predicting material behavior. Incorporating multi-length scale (nonlocal) models into phase transformation simulations offers a promising avenue to address these shortcomings. Other motivations to incorporate multi-length scales in the simulations of phase transformation in steels can be listed as follows:

- Steel microstructures exhibit a hierarchical organization spanning from the atomic to the macroscopic level. Phase transformations involve intricate interactions between defects, grain boundaries, dislocations, and other microstructural features. Traditional models typically focus on a single-length scale, overlooking the collective influence of these features. Nonlocal models offer a holistic approach by capturing the spatial interactions across multiple length scales, thereby providing a more accurate representation of material behavior during phase transformations.
- Incorporating nonlocal models enables a more comprehensive description of phase transformation kinetics and microstructural evolution. By accounting for the influence of neighboring microstructural elements, these models accurately capture phenomena such as strain localization, heterogeneous nucleation, and interface migration. Consequently, they offer improved predictive capabilities for various aspects of phase transformations, including phase fractions, grain size distribution, and mechanical properties.
- Microstructural features significantly influence the mechanical properties of steels. Nonlocal models facilitate a deeper understanding of the intricate relationships between microstructure and mechanical behavior during phase transformations. By accurately predicting the evolution of microstructural features, such as grain size, morphology, and orientation, these models enable researchers to elucidate the underlying mechanisms governing mechanical properties, including strength, toughness, and ductility.
- Phase transformation kinetics and microstructural evolution play a crucial role in determining the final properties of steel components. Nonlocal models provide insights into the influence of processing parameters, such as temperature, cooling rate, and deformation, on phase transformation behavior. By incorporating these models into process simulations, engineers can optimize processing conditions to achieve desired microstructures and properties, thereby enhancing the performance and reliability of steel products.

The integration of Leblond et al.'s [11, 12] model within the finite element analysis (FEA) framework is a pivotal development. When applied to phase transformations in metals, FEA combined with the mixed work-hardening isotropic-kinematic model enables to gain insights into the deformation and stress distribution within materials as they undergo phase changes. This can facilitate the optimization of material selection and the design of components with enhanced performance and durability. This opportunity will be taken to simplify and rationalize the numerical implementation of this behavior for the other types of hardening (namely, ideal perfect plasticity, isotropic hardening, and kinematic hardening). First, in fact, the numerical implementation presents some unnecessary complications, such as the use of a semi-implicit algorithm, whereas a totally explicit, much simpler, algorithm does not lead to a significant degradation of the precision. Second, various additional effects have been introduced into the modeling (e.g., restoration or the memory of work hardening during transformations, effect of large transformations), and their numerical implementation not always being carried out in the same mind as the initial (isotropic hardening) numerical implementation (usually for the sake of simplicity). A general "grooming" therefore seems desirable.

Recently, some new needs appeared concerning the possibility of a mixed work-hardening isotropic-kinematic in the modeling of the plastic behavior of metals during phase transformation developed by Leblond et al. [11, 12]. The objective of this work is to provide a comprehensive description, without too much emphasizing the theoretical aspects, of Leblond et al.'s [11, 12] modeling of transformation plasticity approach and its numerical implementation within the framework of finite element analysis. We will enhance the model proposed

by Leblond et al. [11, 12] to incorporate the intricate mechanisms of mixed isotropic/kinematic hardening. The augmentation entails introducing two characteristic length scales, accompanied by their respective nonlocal variables, which are intricately tied to the effective plastic deformation experienced within both phases. This addition serves the purpose of rectifying the post-bifurcation ill-posedness of the model and ensuring mesh sensitivity concerning the finite element results relative to the mesh utilized.

The remainder of the paper unfolds in the subsequent sections as follows:

1. In Section 1, a comprehensive overview of the constitutive equations proposed by Leblond et al. [11, 12] and its non-local extension are presented, outlining their constitutive model for phase transformation.
2. Moving forward to Section 2, a detailed account of the numerical implementation of this model into a finite element code is provided.
3. Finally, Section 3 showcases the practical application of the model by presenting numerical predictions for a phase transformation scenario involving A.508 cl. 3 and A533 low-alloy steels. The obtained results not only affirm the robustness of the implemented numerical framework but also underscore the model's efficiency in accurately predicting phase transformation phenomena in steels.

## 2. Thermo-plasticity behavior for a mixed isotropic-kinematic hardening

Let us begin for the sake of completeness by recalling the model of plastic behavior with mixed work hardening used in the standard finite element codes, in the absence of phase transformation. We consider the general case of a variable temperature and large deformations.

Let $\sigma_0(T)$ be the initial limit of elasticity, before work hardening, function only of the temperature $T$. Let $\sigma(\varepsilon_{eq}, T)$ be the stress observed in an initial tensile test at the temperature $T$, function of this temperature and of the cumulated plastic deformation $\varepsilon_{eq}$. Let

$$\overline{\sigma}(\varepsilon_{eq}, T) \equiv \sigma(\varepsilon_{eq}, T) - \sigma_0(T), \tag{1}$$

the part of this stress coming from work hardening. Finally, let $p$ be the proportion of work hardening, which is of an isotropic nature.

The limit of elasticity is therefore

$$\sigma^Y(\varepsilon_{eq}, T) \equiv \sigma_0(T) + p\overline{\sigma}(\varepsilon_{eq}, T). \tag{2}$$

The yield criterion is then written as

$$\sigma_{eq} \equiv \left[ \frac{3}{2}(\underline{\underline{s}} - \underline{\underline{a}}) : (\underline{\underline{s}} - \underline{\underline{a}}) \right]^{\frac{1}{2}} \leq \sigma^Y(\varepsilon_{eq}, T), \tag{3}$$

where $\underline{\underline{s}}$ denotes the deviatoric stress. The evolution equation of the center $\underline{\underline{a}}$ of the domain of elasticity is

$$\overset{\triangledown}{\underline{\underline{a}}} \equiv \dot{\underline{\underline{a}}} + \left( \dot{\underline{\underline{a}}} \right)_{GT} = \frac{2}{3}(1-p)\frac{\partial \overline{\sigma}}{\partial \varepsilon_{eq}}(\varepsilon_{eq}, T)\underline{\underline{d}}^p + \frac{1}{\overline{\sigma}}\frac{\partial \overline{\sigma}}{\partial T}(\varepsilon_{eq}, T)\underline{\underline{a}}\dot{T}. \tag{4}$$

In this equation, $\overset{\triangledown}{\underline{\underline{a}}}$ denotes the objective derivative of $a$ chosen (e.g., those of Jaumann or Molinari) and $\left( \dot{\underline{\underline{a}}} \right)_{GT}$ the part, in the expression of this objective derivative, due to large deformations. In addition, $\underline{\underline{d}}^p$ denotes the plastic strain rate (Eulerian). Finally, for the record, the plastic constitutive law is the same as usual:

$$\underline{\underline{d}}^p = \frac{3}{2}\frac{\dot{\varepsilon}_{eq}}{\sigma_{eq}}(\underline{\underline{s}} - \underline{\underline{a}}), \qquad \dot{\varepsilon}_{eq} = \left( \frac{2}{3}\underline{\underline{d}}^p : \underline{\underline{d}}^p \right)^{\frac{1}{2}}. \tag{5}$$

## 3. Plastic behavior during phase transformation in the case of mixed isotropic-kinematic hardening

We will omit the intricacies of the homogenization approach leading to the macroscopic equations of plastic behavior during phase transformations in this section. For a comprehensive understanding of this derivation,
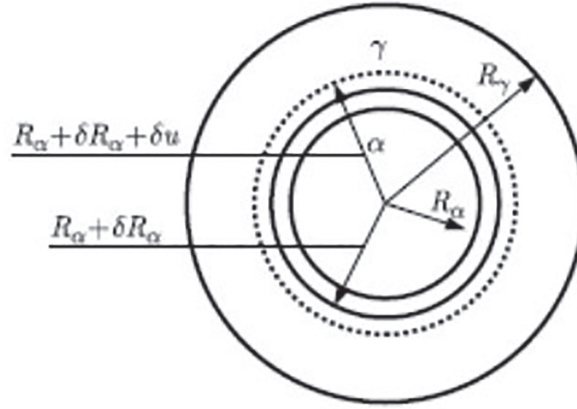
**Figure 1.** Geometry considered by Leblond et al. to illustrate phase transformation of austenitic nuclei [11, 12].

interested readers may refer to the works of Leblond et al. [11, 12]. Additionally, detailed summaries are provided in the Appendices at the end of this manuscript, covering the cases of isotropic and kinematic hardening separately. For the mixed isotropic/kinematic hardening case, we will briefly outline the main constitutive equations of the model, without delving into the technical details of their derivation.

### 3.1. Generalities

Leblond's model is derived from a micromechanical analysis of stress and strain fields in austenitic spherical nuclei during continuous cooling. It focuses on the growth of a spherical product phase core at the center of these nuclei. The model describes the evolution of radii ($R_\gamma$ and $R_\alpha$) representing the parent and product phases, respectively, see Figure 1. $R_\alpha$ starts from zero, progressively increasing during transformation until it equals $R_\gamma$. The model accounts for positive volume changes during transformation, leading to a shift in point locations. Leblond emphasizes that the macroscopic plastic strain rate during phase transformation under external loading is solely influenced by the shape variation of each phase. This conclusion is underpinned by the author's assumption that the impact of local anisotropy resulting from slight differences in elastic parameters between phases is negligible compared to the stresses and deformations caused by volume variations.

The parent phase ($\gamma$) is denoted with an index of 1, and the daughter phase $\alpha$ with an index of 2; $z$ denotes the proportion of daughter phase ($\dot{z}$). We denote $\overline{\sigma}_i(\varepsilon_i^{eff}, T)$ the part coming from the work hardening in the stress observed in a simple tensile test, carried out on a sample of pure phase $i$. This quantity is a function of the effective plastic strain *eff* of the phase $i$, which may differ from the equivalent strain due to the phenomena of memory and restoration of work hardening during the transformations. We denote $\sigma_i^Y(\varepsilon_i^{eff}, T)$ the limit of elasticity of phase $i$, given by a formula analogous to equation (2) (with $\sigma_i^0$ and $\overline{\sigma}_i$ instead of $\overline{\sigma}_i$ and $\sigma_0$). We denote $\underline{\underline{a}}_i$ the center of the elasticity domain of phase $i$.

Finally, the overall limit stress is given by the formula:

$$\sigma^Y(\varepsilon_1^{eff}, \varepsilon_2^{eff}, z, T) = [1 - f(z)]\sigma_1^Y(\varepsilon_1^{eff}, T) + f(z)\sigma_2^Y(\varepsilon_2^{eff}, T). \tag{6}$$

### 3.2. General relations: case where the stress is less than the yield limit

This case is defined by the condition

$$\sigma_{eq} < \sigma^Y, \quad \sigma_{eq} \equiv \left[\frac{3}{2}(\underline{\underline{s}} - \underline{\underline{a}}) : (\underline{\underline{s}} - \underline{\underline{a}})\right]^{\frac{1}{2}}, \quad \underline{\underline{a}} \equiv (1 - z)\underline{\underline{a}}_1 + z\underline{\underline{a}}_2. \tag{7}$$

The other part of the plastic strain rate corresponding to the plasticity of transformation is written as:

$$\underline{\underline{d}}^{pt} = -3\frac{\varepsilon_2^{th}(T) - \varepsilon_1^{th}(T)}{\sigma_1^Y(\varepsilon_1^{eff}, T)} h\left(\frac{\sigma_{eq}}{\sigma^Y}\right)(\ln z)(\underline{\underline{s}} - \underline{\underline{a}}_1)\dot{z}, \tag{8}$$

where $\varepsilon_i^{th}(T)$ is the thermal deformation of the phase $i$. The part of the rate of plastic deformation corresponding to the plastic plasticity is decomposed into two terms, one, $\underline{\underline{d}}_\sigma^{pc}$ coming from the variations of $\underline{\sigma}$ and the other, $\underline{\underline{d}}_T^{pc}$, coming from the variations of $T$ is given by:

$$\underline{\underline{d}}_\sigma^{pc} = \frac{3}{2} \frac{1-z}{\sigma_1^Y(\varepsilon_1^{eff}, T)} \frac{g(z)}{E} (\underline{\underline{s}} - \underline{\underline{a}}_1)(\dot{\sigma}_1^{eq})_s, \tag{9}$$

$$(\dot{\sigma}_1^{eq})_s \equiv \frac{3}{2\sigma_1^{eq}} (\underline{\underline{s}} - \underline{\underline{a}}_1) : \overset{\triangledown}{\underline{\underline{s}}}, \quad \sigma_1^{eq} \equiv \left[ \frac{3}{2} (\underline{\underline{s}} - \underline{\underline{a}}_1) : (\underline{\underline{s}} - \underline{\underline{a}}_1) \right]^{\frac{1}{2}}, \tag{10}$$

$$\underline{\underline{d}}_T^{pc} = 3 \frac{\alpha_1 - \alpha_2}{\sigma_1^Y(\varepsilon_1^{eff}, T)} z(\ln z)(\underline{\underline{s}} - \underline{\underline{a}}_1)\dot{T}, \tag{11}$$

where $\alpha_i$ denotes the coefficient of the thermal dilatation of phase $i$.

The evolution equations of the effective plastic deformation of the phases are as follows:

$$\dot{\varepsilon}_1^{eff} = -2 \frac{\varepsilon_1^{th}(T) - \varepsilon_2^{th}(T)}{1-z} h\left(\frac{\sigma_{eq}}{\sigma^Y}\right)(\ln z)\dot{z} + \frac{g(z)}{E}(\dot{\sigma}_1^{eq})_s +$$
$$2\frac{\alpha_1 - \alpha_2}{1-z} z(\ln z)\dot{T}, \tag{12}$$

$$\dot{\varepsilon}_2^{eff} = \frac{\dot{z}}{z}\varepsilon_2^{eff} + \theta\frac{\dot{z}}{z}\dot{\varepsilon}_1^{eff}, \tag{13}$$

where $\theta$ denotes the memory coefficient of the work hardening during the transformation ($\theta = 0$ means that the hardening of the mother phase is completely forgotten by the daughter phase during the transformation, $\theta = 1$, that this work hardening is, on the contrary, entirely transferred to the daughter phase ). Finally, the evolution equations of the centers of the elasticity domain of the phases are as follows:

$$\overset{\triangledown}{\underline{\underline{a}}}_1 \equiv \underline{\underline{\dot{a}}}_1 + (\underline{\underline{\dot{a}}}_1)_{GT} = \frac{2}{3} \frac{1-p}{1-z} \frac{\partial \overline{\sigma}_1}{\partial \varepsilon_1^{eff}}(\varepsilon_1^{eff}, T)(\underline{\underline{d}}^{pt} + \underline{\underline{d}}_\sigma^{pc} + \underline{\underline{d}}_T^{pc}) +$$
$$\frac{1}{\overline{\sigma}_1} \frac{\partial \overline{\sigma}_1}{\partial T}(\varepsilon_1^{eff}, T)\underline{\underline{a}}_1 \dot{T}, \tag{14}$$

$$\overset{\triangledown}{\underline{\underline{a}}}_2 \equiv \underline{\underline{\dot{a}}}_2 + (\underline{\underline{\dot{a}}}_2)_{GT} = -\frac{\dot{z}}{z}\underline{\underline{a}}_2 + \theta\frac{\dot{z}}{z}\underline{\underline{a}}_1 + \frac{1}{\overline{\sigma}_2} \frac{\partial \overline{\sigma}_2}{\partial T}(\varepsilon_2^{eff}, T)\underline{\underline{a}}_2 \dot{T}. \tag{15}$$

### 3.3. General relations: case where the stress equals the yield limit

This case is defined by the condition

$$\sigma_{eq} = \sigma^Y, \tag{16}$$

where $\sigma_{eq}$ is always defined by the relations equation (7). The flow rule is then

$$\underline{\underline{d}}^p = \frac{3}{2} \frac{\dot{\varepsilon}_{eq}}{\sigma_{eq}}(\underline{\underline{s}} - \underline{\underline{a}}) \qquad \left(\text{with } \dot{\varepsilon}_{eq} = \left(\frac{2}{3}\underline{\underline{d}}_p : \underline{\underline{d}}_p\right)^{\frac{1}{2}}\right). \tag{17}$$

The evolution equations of the work hardening are written as follows:

$$\dot{\varepsilon}_1^{eff} = \dot{\varepsilon}_{eq}, \tag{18}$$

$$\dot{\varepsilon}_2^{eff} = \dot{\varepsilon}_{eq} - \frac{\dot{z}}{z}\varepsilon_2^{eff} + \theta\frac{\dot{z}}{z}\dot{\varepsilon}_1^{eff}, \tag{19}$$

$$\overset{\triangledown}{\underline{\underline{a}}}_1 = \frac{2}{3}(1-p)\frac{\partial\overline{\sigma_1}}{\partial\varepsilon_1^{eff}}(\varepsilon_1^{eff}, T)\underline{\underline{d}}^p + \frac{1}{\overline{\sigma}_1}\frac{\partial\overline{\sigma_1}}{\partial T}(\varepsilon_1^{eff}, T)\underline{\underline{a}}_1\dot{T}, \tag{20}$$

$$\overset{\triangledown}{\underline{\underline{a}}}_2 = \frac{2}{3}(1-p)\frac{\partial\overline{\sigma_2}}{\partial\varepsilon_2^{eff}}(\varepsilon_2^{eff}, T)\underline{\underline{d}}^p + \frac{1}{\overline{\sigma}_2}\frac{\partial\overline{\sigma_2}}{\partial T}(\varepsilon_2^{eff}, T)\underline{\underline{a}}_2\dot{T} - \frac{\dot{z}}{z}\underline{\underline{a}}_2 + \theta\frac{\dot{z}}{z}\underline{\underline{a}}_1. \tag{21}$$

## 4. Adding non-local effects

The inclusion of non-local effects within the phase transformation component of a phase transformation plasticity model involves considering the nature of phase transformations and the potential influence of distant points on the transformation process. Below are several reasons to justify this inclusion:

- *Microstructural influence.* Phase transformations often involve changes in the material's microstructure, such as the formation or dissolution of precipitates, grain boundary migration, or the nucleation and growth of new phases. These microstructural changes can have far-reaching effects beyond the immediate vicinity of the transformation front, impacting the behavior of neighboring regions.
- *Thermal effects*: Phase transformations are often accompanied by significant thermal effects, such as the release or absorption of latent heat. These thermal effects can lead to temperature gradients within the material, which in turn can influence the kinetics of phase transformations in distant regions.
- *Mechanical interactions*: Mechanical stresses generated during phase transformations can propagate through the material, affecting the deformation behavior of neighboring regions. This mechanical interaction can result in non-local effects on both the phase transformation kinetics and the plastic deformation behavior.
- *Diffusion and transport.* Diffusion of species or vacancies plays a crucial role in many phase transformation processes. The transport of diffusing species or vacancies can lead to non-local effects, influencing the kinetics of phase transformations over larger length scales.
- *Experimental observations*: Experimental studies often reveal non-local effects during phase transformations, such as the formation of diffusion bands, compositional gradients, or microstructural heterogeneities across the material. These observations suggest that the influence of distant points on phase transformations cannot be ignored.
- *Pathological post-bifurcation mesh dependency with local phase transformation models.* This refers to a specific type of mesh-dependency issue that arises after a bifurcation or critical point in a numerical simulation. In such cases, the behavior of the solution becomes highly sensitive to the mesh resolution, often leading to non-physical or unstable results. This phenomenon is particularly challenging because it can significantly affect the accuracy and reliability of the simulation results, making it difficult to obtain meaningful predictions. Below is a more detailed explanation of pathological post-bifurcation mesh dependency and how it can occur. In many physical systems, bifurcation points mark significant changes in the behavior of the solution. These points often correspond to critical thresholds or instabilities where the system undergoes a qualitative change in its dynamics. Before the bifurcation point, the solution may converge smoothly and accurately with increasing mesh resolution. However, after the bifurcation point, the behavior of the solution becomes highly sensitive to the mesh resolution. Small changes in the mesh can lead to significant variations in the solution, and the solution may exhibit non-physical oscillations, instability, or divergence.

To account for non-local effects in the model, we decide to include these effects on the evolution equations of the effective plastic deformation of the mother and daughter phases.

By incorporating non-local effects into the phase transformation component of the model, we can better capture these complex interactions and improve the model's ability to predict the behavior of materials undergoing phase transformation plasticity under realistic conditions. This leads to more accurate simulations and a deeper understanding of the underlying physics governing phase transformations in materials.

In certain applications, especially those involving high stress and/or strain gradients, the effective plastic deformation evolution equation can undergo a process of delocalization. In this context, we define local rates of

effective plastic growth increase due to the accumulation of plastic deformation. The local rates are determined by formula (12) and (13). The true non-local growth rate is then computed using the convolution formulas presented below:

$$\dot{\varepsilon}_1^{eff}(\mathbf{x}) = \frac{1}{C(\mathbf{x})} \int_\Omega \dot{\varepsilon}_{1,loc}^{eff}(\mathbf{y}) \chi_1(\mathbf{x} - \mathbf{y}) d\Omega_y \, ,$$

$$\dot{\varepsilon}_2^{eff}(\mathbf{x}) = \frac{1}{C(\mathbf{x})} \int_\Omega \dot{\varepsilon}_{2,loc}^{eff}(\mathbf{y}) \chi_2(\mathbf{x} - \mathbf{y}) d\Omega_y \, , \tag{22}$$

$$C(\mathbf{x}) = \int_\Omega \chi(\mathbf{x} - \mathbf{y}) d\Omega_\mathbf{y} \, .$$

Here, $\Omega$ denotes the studied domain and $\chi_1, \chi_2$ are weighting functions, which we take to be Gaussian for practical purpose:

$$\chi_1(\mathbf{z}) = exp\left(\frac{-|\mathbf{z}|^2}{l_1^2}\right), \quad \chi_2(\mathbf{z}) = exp\left(\frac{-|\mathbf{z}|^2}{l_2^2}\right), \tag{23}$$

where $l_1$ and $l_2$ serve as characteristic lengths, representing micro-structural effects and they play a role similar to the minimum mesh size. It is worth noting that this delocalization study has been extensively explored in the context of damage modeling in studies by Leblond et al. [13] , Enakoutsa and colleagues [14–24], and in many other works including the pioneering work of Pijaudier-Cabot and Bazant [25], but in the context of modeling of concrete materials.

## 5. Numerical implementation of the constitutive relations of the model

The selection of an algorithm for each equation introduces the challenge of deciding between explicit, implicit, or semi-implicit methods. The choices presented here, although not entirely aligning with previous decisions, stem from thoughtful considerations:

a.   An explicit algorithm is favored when it allows for a streamlined digitization process without a substantial sacrifice in accuracy. The emphasis is on simplifying the numerical implementation, making it computationally efficient while maintaining an acceptable level of precision. This choice is particularly relevant in scenarios where computational efficiency is paramount, and the simplification of the numerical scheme does not compromise the overall solution accuracy.

b.   An implicit algorithm is favored concerning the direction of the plastic flow, as dictated by the stress deviator. This preference aligns with standard practices in finite element codes, ensuring consistency with widely adopted programming conventions. Implicit methods are known for their stability and unconditional convergence, making them suitable for capturing the plastic flow behavior with numerical robustness.

c.   A semi-implicit algorithm is favored when there is a substantial improvement in accuracy, or even if there isn't, as long as it doesn't significantly complicate the numerical implementation. This choice reflects a balance between accuracy enhancement and computational efficiency, considering scenarios where a fully implicit approach may be overly complex while maintaining the advantages of implicit methods in specific aspects. The decision to opt for a semi-implicit approach acknowledges the nuanced trade-off between accuracy and computational cost, allowing for a pragmatic solution that suits the specific requirements of the problem at hand.

The algorithmic choices made in this context are driven by a nuanced understanding of the trade-offs between computational efficiency, solution accuracy, and the compatibility of the chosen approach with standard programming practices in finite element codes.

## 5.1. Case where the yield limit is not reached

The partition of the deviator of the increment of the total strain (thermal part subtracted) between the times $t$ and $t + \Delta t$ is written as

$$\Delta \underline{e} = \Delta \underline{e}^e + \Delta \underline{\varepsilon}^p = \Delta \underline{e}^e + (\Delta \underline{\varepsilon}^p)' + (\Delta \underline{\varepsilon}^p)'', \tag{24}$$

where the term $((\Delta \underline{\varepsilon}^p)')$ corresponds to $(\underline{d}_{pt} + \underline{d}_T^{pc})\Delta t$ and $((\Delta \underline{\varepsilon}^p)'')$ to $(\underline{d}_\sigma^{pc})\Delta t$. The expressions of these terms are the following, where $F$ denotes the function of the von Mises $\left(F(\underline{X}) = \left(\frac{3}{2}\underline{X} : \underline{X}\right)^{1/2}\right)$:

$$(\Delta \underline{\varepsilon}^p)' = \frac{A}{2} \left[ 1 + \frac{F(\underline{s} - \underline{a}_1)}{F(\underline{s} + \Delta \underline{s} - \underline{a}_1 - \Delta \underline{a}_1)} \right] (\underline{s} + \Delta \underline{s} - \underline{a}_1 - \Delta \underline{a}_1), \tag{25}$$

$$(\Delta \underline{\varepsilon}^p)'' = \frac{B}{2} \left[ 1 + \frac{F(\underline{s} - \underline{a}_1)}{F(\underline{s} + \Delta \underline{s} - \underline{a}_1 - \Delta \underline{a}_1)} \right] (\Delta \sigma_1^{eq})_s (\underline{s} + \Delta \underline{s} - \underline{a}_1 - \Delta \underline{a}_1). \tag{26}$$

In the expression (25), $A$ is given by:

$$
\begin{aligned}
A = & -3 \frac{\varepsilon_2^{th}(T) - \varepsilon_1^{th}(T) + \varepsilon_2^{th}(T + \Delta T) - \varepsilon_1^{th}(T + \Delta T)}{\sigma_1^Y(\varepsilon_1^{eff}, T) + \sigma_1^Y(\varepsilon_1^{eff}, T + \Delta T)} h\left(\frac{\sigma_{eq}}{\sigma^Y}\right) \times \\
& \{(z + \Delta z)[\ln(z + \Delta z) - 1] - z(\ln z - 1)\} + \\
& 3 \frac{\varepsilon_1^{th}(T + \Delta T) - \varepsilon_1^{th}(T) + \varepsilon_2^{th}(T + \Delta T) - \varepsilon_2^{th}(T)}{\sigma_1^Y(\varepsilon_1^{eff}, T) + \sigma_1^Y(\varepsilon_1^{eff}, T + \Delta T)} \times \\
& [z \ln z + (z + \Delta Z)\ln(z + \Delta z)].
\end{aligned}
\tag{27}
$$

The term $h(\bar{\sigma}_{eq}/\sigma^Y)$ in this expression is discretized explicitly. Moreover, the term comes from an exact integration of $\ln(z)$ between $z$ and $z + \Delta z$ in equation (8), the other terms being considered constant. Numerical experiments have shown the importance of such exact integration to conveniently reproduce stress dilatometry tests.

The quantity $B$ in equation (26) is given by:

$$B = 3 \frac{(1 - z)g(z) + (1 - z - \Delta z)g(z + \Delta z)}{\left[\sigma_1^Y(\varepsilon_1^{eff}, T) + \sigma_1^Y(\varepsilon_1^{eff}, T + \Delta T)\right][E(T) + E(T + \Delta T)]}. \tag{28}$$

In addition, $(\Delta \sigma_1^{eq})_s$ is given by:

$$(\Delta \sigma_1^{eq})_s = \frac{3}{2F(\underline{s} + \Delta \underline{s} - \underline{a}_1 - \Delta \underline{a}_1)}(\underline{s} + \Delta \underline{s} - \underline{a}_1 - \Delta \underline{a}_1) : (\Delta \underline{s})_{OBJ}, \tag{29}$$

where $(\Delta \underline{s})_{OBJ}(\equiv \underline{\check{s}})$ is the objective part of the deviatoric stress rate

$$(\Delta \underline{s})_{OBJ} \equiv \Delta \underline{s} + (\Delta \underline{s})_{GT}. \tag{30}$$

The hypo-elasticity law is given by:

$$(\Delta \underline{s})_{OBJ}(= \Delta \underline{s} + (\Delta \underline{s})_{GT}) = 2\mu \Delta \underline{e}^e + (\Delta \underline{s})_T, \tag{31}$$

where $\mu$ denotes the shear coefficient at the time $t + \Delta t$ (this notation is used here rather than the more logical notation $\mu + \Delta \mu$ to simplify the writing) and $(\Delta \underline{\underline{s}})_T$ the part of $\Delta \underline{\underline{s}}$ coming from the variation of the temperature (via its influence on $\mu$.) The evolution equation of $\varepsilon_1^{eff}$ is discretized as the following equation:

$$\Delta \varepsilon_1^{eff} = \frac{2}{3} \frac{\sigma_1^Y(\varepsilon_1^{eff}, T) + \sigma_1^Y(\varepsilon_1^{eff}, T + \Delta T)}{(1 - z) + (1 - z + \Delta z)} [A + B(\Delta \sigma_1^{eq})_s]. \tag{32}$$

The equation of $\varepsilon_1^{eff}$ is written in the form $\frac{d}{dt}\left(z \varepsilon_1^{eff}\right) = \theta \varepsilon_1^{eff} \dot{z}$ before being discretized by

$$\Delta(z \varepsilon_2^{eff}) \equiv (z + \Delta z)(\varepsilon_2^{eff} + \Delta \varepsilon_2^{eff}) - z \varepsilon_2^{eff} = \theta \varepsilon_1^{eff} \Delta z. \tag{33}$$

Similarly, the evolution equations of $\underline{\underline{a}}_1$ and $\underline{\underline{a}}_2$ are discretized as follows:

$$(\Delta \underline{\underline{a}}_1)_{OBJ} \equiv \Delta \underline{\underline{a}}_1 + (\Delta \underline{\underline{a}}_1)_{GT} = \frac{2}{3} \frac{1 - p}{1 - z - \Delta z/2} \frac{\partial \overline{\sigma}_1}{\partial \varepsilon_1^{eff}}(\varepsilon_1^{eff}, T + \Delta T)$$

$$\left[(\Delta \underline{\underline{\varepsilon}}^p)' + \varepsilon^p)''\right] + (\Delta \underline{\underline{a}}_1)_T$$

$$\Longrightarrow \Delta \underline{\underline{a}}_1 = \frac{2}{3} \frac{1 - p}{1 - z - \Delta z/2} \frac{\partial \overline{\sigma}_1}{\partial \varepsilon_1^{eff}}(\varepsilon_1^{eff}, T + \Delta T)\left[(\Delta \underline{\underline{\varepsilon}}^p)' + (\Delta \underline{\underline{\varepsilon}}^p)''\right] \tag{34}$$

$$- (\Delta \underline{\underline{a}}_1)_{GT} + (\Delta \underline{\underline{a}}_1)_T.$$

Note in equation (34) the use of the hardening slope $\frac{\partial \overline{\sigma}_1}{\partial \varepsilon_1^{eff}}(\varepsilon_1^{eff}, T + \Delta T)$ instead of the secant as previously. The interest of this replacement is to lead to an explicit resolution not requiring iterations on the parameter of work hardening $\varepsilon_1^{eff} + \Delta \varepsilon_1^{eff}$; it is licit insofar as there are no criteria to be satisfied exactly at the time $t + \Delta t$ (it will not be the same if the yield limit is reached). Moreover, note that the terms $(\Delta \underline{\underline{a}}_i)_{GT}$ and $(\Delta \underline{\underline{a}}_i)_T$ are discretized in an explicit way and therefore known from the beginning.

Now let us move on to solving these equations; the principal unknowns used are

$$\Delta(z \underline{\underline{a}}_2) \equiv (z + \Delta z)(\underline{\underline{a}}_2 + \Delta \underline{\underline{a}}_2) - z \underline{\underline{a}}_2 = \theta \underline{\underline{a}}_1 \Delta z - z(\Delta \underline{\underline{a}}_2)_{GT} + z(\Delta \underline{\underline{a}}_2)_T. \tag{35}$$

Combining equations (24) and (31), we get

$$X = F(\underline{\underline{s}} + \Delta \underline{\underline{s}} - \underline{\underline{a}}_1 - \Delta \underline{\underline{a}}_1), \quad Y = (\Delta \sigma_1^{eq})_s, \tag{36}$$

$$\Delta \underline{\underline{s}} = 2\mu \Delta \underline{\underline{e}}^e - (\Delta \underline{\underline{s}})_{GT} + (\Delta \underline{\underline{s}})_T \quad \Longrightarrow$$

$$\underline{\underline{s}} + \Delta \underline{\underline{s}} \equiv (\underline{\underline{s}} + \Delta \underline{\underline{s}})^{el} - 2\mu \left[(\Delta \underline{\underline{\varepsilon}}^p)' + (\Delta \underline{\underline{\varepsilon}}^p)''\right], \tag{37}$$

$$(\underline{\underline{s}} + \Delta \underline{\underline{s}})^{el} \equiv \underline{\underline{s}} + 2\mu \Delta \underline{\underline{e}} - (\Delta \underline{\underline{s}})_{GT} + (\Delta \underline{\underline{s}})_T, \tag{38}$$

where $(\underline{\underline{s}} + \Delta \underline{\underline{s}})^{el}$, known quantity, is the deviatoric stress at $t + \Delta t$ elastically calculated, that is by considering the deviatoric part of the increment of the total strain $\Delta \underline{\underline{e}}$ (with the thermal part not being accounted for) as purely elastic. Adding $-\underline{\underline{a}}_1 - \Delta \underline{\underline{a}}_1$ to the two sides of equation (37) and taking into account equation (34), we get

$$\underline{\underline{s}} + \Delta \underline{\underline{s}} - \underline{\underline{a}}_1 - \Delta \underline{\underline{a}}_1 = (\underline{\underline{s}} + \Delta \underline{\underline{s}})^{el} - \underline{\underline{a}}_1 - \Delta \underline{\underline{a}}_1 - 2\mu \left[(\Delta \underline{\underline{\varepsilon}}^p)' + (\Delta \underline{\underline{\varepsilon}}^p)''\right]$$

$$= (\underline{\underline{s}} + \Delta \underline{\underline{s}})^{el} - \underline{\underline{a}}_1 + (\Delta \underline{\underline{a}}_1)_{GT} - (\Delta \underline{\underline{a}}_1)_T$$

$$- \left[2\mu + \frac{2}{3} \frac{1 - p}{1 - z - \Delta z/2} \frac{\partial \overline{\sigma}_1}{\partial \varepsilon_1^{eff}}(\varepsilon_1^{eff}, T + \Delta T)\right] \times$$

$$\left[(\Delta \underline{\underline{\varepsilon}}^p)' + (\Delta \underline{\underline{\varepsilon}}^p)''\right]$$

which, by setting

$$\underline{\underline{s}}^* \equiv (\underline{\underline{s}} + \Delta\underline{\underline{s}})^{el} - \underline{\underline{a}}_1 + (\Delta\underline{\underline{a}}_1)_{GT} - (\Delta\underline{\underline{a}}_1)_T \tag{39}$$

is equivalent to

$$H \equiv \frac{1-p}{1-z-\Delta z/2} \frac{\partial\overline{\sigma}_1}{\partial\varepsilon_1^{eff}}(\varepsilon_1^{eff}, T + \Delta T) \tag{40}$$

(these quantities are known):

$$\underline{\underline{s}} + \Delta\underline{\underline{s}} - \underline{\underline{a}}_1 - \Delta\underline{\underline{a}}_1 = \underline{\underline{s}}^* - 2\left(\mu + \frac{H}{3}\right)\left[(\Delta\underline{\underline{\varepsilon}}^p)' + (\Delta\underline{\underline{\varepsilon}}^p)''\right].$$

According to equations (25) and (26) and the notations equation (36), we get

$$(\Delta\underline{\underline{\varepsilon}}^p)' + (\Delta\underline{\underline{\varepsilon}}^p)'' = \frac{1}{2}(A + BY)\left(1 + \frac{F(\underline{\underline{s}} - \underline{\underline{a}}_1)}{X}\right)(\underline{\underline{s}} + \Delta\underline{\underline{s}} - \underline{\underline{a}}_1 - \Delta\underline{\underline{a}}_1), \tag{41}$$

which by reporting in the previous equation reads

$$\underline{\underline{s}} + \Delta\underline{\underline{s}} - \underline{\underline{a}}_1 - \Delta\underline{\underline{a}}_1 = \underline{\underline{s}}^* - \left(\mu + \frac{H}{3}\right)(A + BY)\left(1 + \frac{F(\underline{\underline{s}} - \underline{\underline{a}}_1)}{X}\right)(\underline{\underline{s}} + \Delta\underline{\underline{s}} - \underline{\underline{a}}_1 - \Delta\underline{\underline{a}}_1)$$

$$\Rightarrow \left[1 + \left(\mu + \frac{H}{3}\right)(A + BY)\left(1 + \frac{F(\underline{\underline{s}} - \underline{\underline{a}}_1)}{X}\right)\right](\underline{\underline{s}} + \Delta\underline{\underline{s}} - \underline{\underline{a}}_1 - \Delta\underline{\underline{a}}_1) = \underline{\underline{s}}^*. \tag{42}$$

This equation implies that the (unknown) tensor $\underline{\underline{s}} + \Delta\underline{\underline{s}} - \underline{\underline{a}}_1 - \Delta\underline{\underline{a}}_1$ is positively parallel to the (unknown) tensor $\underline{\underline{s}}^*$. Thus,

$$\underline{\underline{s}} + \Delta\underline{\underline{s}} - \underline{\underline{a}}_1 - \Delta\underline{\underline{a}}_1 = \frac{X}{F(\underline{\underline{s}}^*)}\underline{\underline{s}}^*, \tag{43}$$

which brings the calculation of the unknown $\underline{\underline{s}} + \Delta\underline{\underline{s}} - \underline{\underline{a}}_1 - \Delta\underline{\underline{a}}_1$ to the same of the norm of $X$. Moreover, by taking the von Mises function of equation (43), we obtain:

$$X + \left(\mu + \frac{H}{3}\right)(A + BY)\left(X + F(\underline{\underline{s}} - \underline{\underline{a}}_1)\right) = F(\underline{\underline{s}}^*)$$

$$\Rightarrow A + BY = \frac{F(\underline{\underline{s}}^*) - X}{\left(\mu + \frac{H}{3}\right)\left(X + F(\underline{\underline{s}} - \underline{\underline{a}}_1)\right)} \tag{44}$$

$$\Leftrightarrow Y = \frac{1}{B}\left[\frac{F(\underline{\underline{s}}^*) - X}{\left(\mu + \frac{H}{3}\right)\left(X + F(\underline{\underline{s}} - \underline{\underline{a}}_1)\right)} - A\right].$$

The unknown quantity $Y$ can now be expressed as a function of the unknown $X$, and it remains to calculate the latter. For this, let us re-express $\underline{\underline{s}} + \Delta\underline{\underline{s}} - \underline{\underline{a}}_1 - \Delta\underline{\underline{a}}_1$ using the equations (30) and (32) as well as the definition equation (40) as:

$$\underline{\underline{s}} + \Delta\underline{\underline{s}} - \underline{\underline{a}}_1 - \Delta\underline{\underline{a}}_1 = \underline{\underline{s}} - (\Delta\underline{\underline{s}})_{GT} + (\Delta\underline{\underline{s}})_{OBJ} - \underline{\underline{a}}_1 - \frac{2}{3}H\left[(\Delta\underline{\underline{\varepsilon}}^p)' + (\Delta\underline{\underline{\varepsilon}}^p)''\right] + (\Delta\underline{\underline{a}}_1)_{GT} - (\Delta\underline{\underline{a}}_1)_T,$$

which, by accounting for equations (41) and (44), reads

$$
\begin{aligned}
\underline{\underline{s}} + \Delta\underline{\underline{s}} - \underline{\underline{a}}_1 - \Delta\underline{\underline{a}}_1 &= \underline{\underline{s}} - (\Delta\underline{\underline{s}})_{GT} - \underline{\underline{a}}_1 + (\Delta\underline{\underline{a}}_1)_{GT} - (\Delta\underline{\underline{a}}_1)_T \\
&\quad - \frac{H}{3}(A + BY)\left(1 + \frac{F(\underline{\underline{s}} - \underline{\underline{a}}_1)}{X}\right)(\underline{\underline{s}} + \Delta\underline{\underline{s}} - \underline{\underline{a}}_1 - \Delta\underline{\underline{a}}_1) + (\Delta\underline{\underline{s}})_{OBJ} \\
&= \underline{\underline{s}} - (\Delta\underline{\underline{s}})_{GT} - \underline{\underline{a}}_1 + (\Delta\underline{\underline{a}}_1)_{GT} - (\Delta\underline{\underline{a}}_1)_T \\
&\quad + \frac{H\left(X - F(\underline{\underline{s}}^*)\right)}{(H + 3\mu)\left(X + F(\underline{\underline{s}} - \underline{\underline{a}}_1)\right)}\left(1 + \frac{F(\underline{\underline{s}} - \underline{\underline{a}}_1)}{X}\right)(\underline{\underline{s}} + \Delta\underline{\underline{s}} - \underline{\underline{a}}_1 - \Delta\underline{\underline{a}}_1) + (\Delta\underline{\underline{s}})_{OBJ}.
\end{aligned}
$$

Contracting this equation with $\frac{3}{2}\underline{\underline{s}}^*$ gives, taking into account the definition equation (29) of $\left(\Delta\sigma_1^{eq}\right)_s \equiv Y$ and the property equation (43),

$$
XF(\underline{\underline{s}}^*) = P + \frac{H\left(X - F(\underline{\underline{s}}^*)\right)}{(H + 3\mu)\left(X + F(\underline{\underline{s}} - \underline{\underline{a}}_1)\right)}\left(X + F(\underline{\underline{s}} - \underline{\underline{a}}_1)\right)F(\underline{\underline{s}}^*) + F(\underline{\underline{s}}^*)Y,
$$

where we assumed that

$$
P \equiv \frac{3}{2}\left(\underline{\underline{s}} - (\Delta\underline{\underline{s}})_{GT} - \underline{\underline{a}}_1 + (\Delta\underline{\underline{a}}_1)_{GT} - (\Delta\underline{\underline{a}}_1)_T\right) : \underline{\underline{s}}^*
$$

($P$ is a known quantity). Multiplying by $(H + 3\mu)\left(X + F(\underline{\underline{s}} - \underline{\underline{a}}_1)\right)$ and accounting for equation (44)

$$
\begin{aligned}
(H + 3\mu)\left(X + F(\underline{\underline{s}} - \underline{\underline{a}}_1)\right)XF(\underline{\underline{s}}^*) &= P(H + 3\mu)\left(X + F(\underline{\underline{s}} - \underline{\underline{a}}_1)\right) \\
&\quad + H\left(X - F(\underline{\underline{s}}^*)\right)\left(X + F(\underline{\underline{s}} - \underline{\underline{a}}_1)\right)F(\underline{\underline{s}}^*) \\
&\quad + \frac{F(\underline{\underline{s}}^*)}{B}\left[3\left(F(\underline{\underline{s}}^*) - X\right) - A(H + 3\mu)\left(X + F(\underline{\underline{s}} - \underline{\underline{a}}_1)\right)\right],
\end{aligned}
$$

which gives after multiplication by $B$ and re-arrangement:

$$
LX^2 + MX + N = 0, \tag{45}
$$

$$
L \equiv 3\mu BF(\underline{\underline{s}}^*), \tag{46}
$$

$$
M \equiv 3\mu BF(\underline{\underline{s}} - \underline{\underline{a}}_1)F(\underline{\underline{s}}^*) + BHF^2(\underline{\underline{s}}^*) + A(H + 3\mu)F(\underline{\underline{s}}^*) - B(H + 3\mu)P. \tag{47}
$$

The roots of this equation are $\frac{1}{2L}\left(-M \pm \sqrt{M^2 - 4LN}\right)$. The choice of the sign in front of the radical is not obvious a priori because as much as it is clear that $L > 0$, $M$ and $N$ can a priori take any sign. However, in practice, the coefficient $B$ is small. We then see from equation (47) that $M > 0$, the $-$ sign in front of the radical then leads to a negative root, which is impossible since the equation is greater than $X \equiv F\left(\underline{\underline{s}} + \Delta\underline{\underline{s}} - \underline{\underline{a}}_1 - \Delta\underline{\underline{a}}_1\right) > 0$, therefore the $+$ sign that must be retained.

$$
\begin{aligned}
N \equiv -3F^2(\underline{\underline{s}}^*) + BHF(\underline{\underline{s}} - \underline{\underline{a}}_1)F^2(\underline{\underline{s}}^*) + A(H + 3\mu)F(\underline{\underline{s}} - \underline{\underline{a}}_1)F(\underline{\underline{s}}^*) - \\
B(H + 3\mu)PF(\underline{\underline{s}} - \underline{\underline{a}}_1),
\end{aligned} \tag{48}
$$

$$X = \frac{1}{2L}\left(-M + \sqrt{M^2 - 4LN}\right). \tag{49}$$

However, even with this choice of signs in front of the radical, the sign of the solution is not clear because it depends on that of $N$, which is not itself clear (even with $B$ small). It is therefore not impossible that equation (49) provides a negative root. In this case, it is better to adopt another algorithm which may be less precise but certainly leads to a positive root. It suffices for this purpose to replace the expressions equations (25) and (26), semi-implicit with respect to the norm of $\underline{s} - \underline{a}_1$, by the implicit expressions:

$$(\Delta\underline{\underline{\varepsilon}}^p)' = A(\underline{\underline{s}} + \Delta\underline{\underline{s}} - \underline{\underline{a}}_1 - \Delta\underline{\underline{a}}_1), \tag{25'}$$

$$(\Delta\underline{\underline{\varepsilon}}^p)'' = B(\Delta\sigma_1^{eq})_s(\underline{\underline{s}} + \Delta\underline{\underline{s}} - \underline{\underline{a}}_1 - \Delta\underline{\underline{a}}_1), \tag{26'}$$

$$L'X^2 + M'X + N' = 0. \tag{45'}$$

We can see that to find these expressions from equations (25) and (26), we shall replace $F(\underline{\underline{s}} - \underline{\underline{a}}_1)$ by $F\left(\underline{\underline{s}} + \Delta\underline{\underline{s}} - \underline{\underline{a}}_1 - \Delta\underline{\underline{a}}_1\right) \equiv X$. We obtain therefore the same equation (45) on $X$ as previously, but by performing this substitution in the expressions (46)–(48) of $L, M, N$, this equation becomes

$$L' = 6\mu BF(\underline{\underline{s}}^*), \tag{45'}$$

$$M' = 2BHF^2(\underline{\underline{s}}^*) + 2A(H + 3\mu)F(\underline{\underline{s}}^*) - 2B(H + 3\mu)P, \tag{46'}$$

$$N = -3F^2(\underline{\underline{s}}^*). \tag{47'}$$

The coefficients $L'$ and $N'$ are here clearly positive and negative, respectively; therefore, the product of the roots $N'/L'$ is negative, so that there are two roots reals, one positive and the other one negative, as desired; the positive root is

$$X = \frac{1}{2L'}\left(-M' + \sqrt{M'^2 - 4L'N'}\right). \tag{48'}$$

Once $X$ is calculated by equation (49), we can deduce $Y$ by equation (44) (eventually by replacing $F(\underline{\underline{s}} - \underline{\underline{a}}_1)$ by $X$), $\underline{\underline{s}} + \Delta\underline{\underline{s}} - \underline{\underline{a}}_1 - \Delta\underline{\underline{a}}_1$ by equation (43), $(\Delta\underline{\underline{\varepsilon}}^p)' + (\Delta\underline{\underline{\varepsilon}}^p)''$ by equation (41) (by replacing again eventually $X$ by $F(\underline{\underline{s}} - \underline{\underline{a}}_1)$), $\underline{\underline{s}} + \Delta\underline{\underline{s}}$ by equation (37). It remains to update the parameter of strain hardening. The variations of $\varepsilon_2^{eff}$ and $\underline{\underline{a}}_2$ are given by equations (32) and (34). The variations of $\varepsilon_2^{eff}$ and and $\underline{\underline{a}}_2$ are obtained from equations (33) and (35) which can be re-written as:

$$\varepsilon_2^{eff}\Delta z + (z + \Delta z)\varepsilon_2^{eff} = \theta\varepsilon_1^{eff}\Delta z \Rightarrow \Delta\varepsilon_2^{eff} = \frac{\Delta z}{z + \Delta z}(-\varepsilon_2^{eff} + \theta\varepsilon_1^{eff}), \tag{50}$$

$$\underline{\underline{a}}_2\Delta z + (z + \Delta z)\Delta\underline{\underline{a}}_2 = \theta\underline{\underline{a}}_1\Delta z - z(\Delta\underline{\underline{a}}_2)_{GT} + z(\Delta\underline{\underline{a}}_2)_T \Rightarrow$$
$$\Delta\underline{\underline{a}}_2 = \frac{1}{z + \Delta z}\left[(-\underline{\underline{a}}_2 + \theta\underline{\underline{a}}_1)\Delta z - z(\Delta\underline{\underline{a}}_2)_{GT} + z(\Delta\underline{\underline{a}}_2)_T\right]. \tag{51}$$

(Let us note that due to the discretization explicit of $\Delta\underline{\underline{a}}_2)_{GT}$ and $(\Delta\underline{\underline{a}}_2)_T$, the variations of $\varepsilon_2^{eff}$ and $\underline{\underline{a}}_2$ can, in fact, be calculated at the beginning, before the calculation of $X$ and $Y$.)

$$\sigma_{eq} + \Delta\sigma_{eq} \equiv F(\underline{\underline{s}} + \Delta\underline{\underline{s}} - \underline{\underline{a}} - \Delta\underline{\underline{a}}) < \sigma^Y + \Delta\sigma^Y. \tag{52}$$

It is finally necessary to verify the stress-limit condition is not reached, defining the case considered. The calculation of $\sigma^Y + \Delta\sigma^Y$ is immediate knowing $\varepsilon_1^{eff} + \Delta\varepsilon_1^{eff}$, $\varepsilon_2^{eff} + \Delta\varepsilon_2^{eff}$, $z + \Delta z$, $T + \Delta T$. Finding the value of $\sigma_{eq} + \Delta\sigma_{eq}$ necessitates to evaluate $(\underline{\underline{s}} + \Delta\underline{\underline{s}} - \underline{\underline{a}} - \Delta\underline{\underline{a}})$. We obtain:

$$\underline{\underline{s}} + \Delta\underline{\underline{s}} - \underline{\underline{a}} - \Delta\underline{\underline{a}} = \underline{\underline{s}} + \Delta\underline{\underline{s}} - (1 - z - \Delta z)(\underline{\underline{a}}_1 + \Delta\underline{\underline{a}}_1) - (z + \Delta z)(\underline{\underline{a}}_2 + \Delta\underline{\underline{a}}_2).$$

All tensors being known here, we deduce $(\underline{\underline{s}} + \Delta\underline{\underline{s}} - \underline{\underline{a}} - \Delta\underline{\underline{a}})$. However, we can calculate this expression before evaluating $\Delta\underline{\underline{a}}_1$ using $X$, $Y$ and the tensors known a priori $\underline{\underline{s}}^\star$, $\left(\Delta\underline{\underline{a}}_1\right)_{GT}$, $\left(\Delta\underline{\underline{a}}_1\right)_T$, and $\Delta\underline{\underline{a}}_2$. Indeed, from equations (34) and (41),

$$\underline{\underline{a}}_1 + \Delta\underline{\underline{a}}_1 = \underline{\underline{a}}_1 + \frac{H}{3}(A + BY)\left(1 + \frac{F(\underline{\underline{s}} - \underline{\underline{a}}_1)}{X}\right)(\underline{\underline{s}} + \Delta\underline{\underline{s}} - \underline{\underline{a}}_1 - \Delta\underline{\underline{a}}_1)$$
$$-(\Delta\underline{\underline{a}}_1)_{GT} + (\Delta\underline{\underline{a}}_1)_T,$$

where we deduce, using the previous expression of $(\underline{\underline{s}} + \Delta\underline{\underline{s}} - \underline{\underline{a}} - \Delta\underline{\underline{a}})$ and equation (43):

$$
\begin{aligned}
\underline{\underline{s}} + \Delta\underline{\underline{s}} - \underline{\underline{a}} - \Delta\underline{\underline{a}} &= \underline{\underline{s}} + \Delta\underline{\underline{s}} - \underline{\underline{a}}_1 - \Delta\underline{\underline{a}}_1 + (z + \Delta z)(\underline{\underline{a}}_1 + \Delta\underline{\underline{a}}_1 - \underline{\underline{a}}_2 - \Delta\underline{\underline{a}}_2) \\
&= \left[1 + (z + \Delta z)\frac{H}{3}(A + BY)\left(1 + \frac{F(\underline{\underline{s}} - \underline{\underline{a}}_1)}{X}\right)\right](\underline{\underline{s}} + \Delta\underline{\underline{s}} - \underline{\underline{a}}_1 - \Delta\underline{\underline{a}}_1) \\
&\quad + (z + \Delta z)(\underline{\underline{a}}_1 - (\Delta\underline{\underline{a}}_1)_{GT} + (\Delta\underline{\underline{a}}_1)_T - \underline{\underline{a}}_2 - \Delta\underline{\underline{a}}_2) \\
&= \left[X + (z + \Delta z)\frac{H}{3}(A + BY)\left(X + F(\underline{\underline{s}} - \underline{\underline{a}}_1)\right)\right]\frac{\underline{\underline{s}}^*}{F(\underline{\underline{s}}^*)} \\
&\quad + (z + \Delta z)(\underline{\underline{a}}_1 - (\Delta\underline{\underline{a}}_1)_{GT} + (\Delta\underline{\underline{a}}_1)_T - \underline{\underline{a}}_2 - \Delta\underline{\underline{a}}_2)
\end{aligned}
\tag{53}
$$

(of course, it is still possible to substitute $X$ with $F(\underline{\underline{s}} - \underline{\underline{a}})$ in this expression).

## 5.2. Case where the limit stress is reached

The discretized equations can be written as:

$$\Delta\underline{\underline{e}} = \Delta\underline{\underline{e}}^e + \Delta\underline{\underline{\varepsilon}}^P, \tag{54}$$

$$\sigma_{eq} + \Delta\sigma_{eq} \equiv F(\underline{\underline{s}} + \Delta\underline{\underline{s}} - \underline{\underline{a}} - \Delta\underline{\underline{a}}) = \sigma^Y(\varepsilon_1^{eff} + \Delta\varepsilon_1^{eff}, \varepsilon_2^{eff} + \Delta\varepsilon_2^{eff}, z + \Delta z, T + \Delta T), \tag{55}$$

$$\Delta\underline{\underline{\sigma}}^P = \frac{3}{2}\frac{\Delta\varepsilon_{eq}}{F(\underline{\underline{s}} + \Delta\underline{\underline{s}} - \underline{\underline{a}} - \Delta\underline{\underline{a}})}(\underline{\underline{s}} + \Delta\underline{\underline{s}} - \underline{\underline{a}} - \Delta\underline{\underline{a}}), \tag{56}$$

$$
\begin{aligned}
\Delta\underline{\underline{s}}_{OBJ} &= \Delta\underline{\underline{s}} + (\Delta\underline{\underline{s}})_{GT} = 2\mu\Delta\underline{\underline{e}}^e + (\Delta\underline{\underline{s}})_T \\
&\Rightarrow \Delta\underline{\underline{s}} = 2\mu\Delta\underline{\underline{e}}^e - (\Delta\underline{\underline{s}})_{GT} + (\Delta\underline{\underline{s}})_T,
\end{aligned}
\tag{57}
$$

$$\Delta\varepsilon_1^{eff} = \Delta\varepsilon_{eq}, \tag{58}$$

$$
\begin{aligned}
\Delta(z\varepsilon_2^{eff}) &= \left(z + \frac{\Delta z}{2}\right)\Delta\varepsilon_{eq} + \theta\varepsilon_1^{eff}\Delta z \Rightarrow \\
\Delta\varepsilon_2^{eff} &= \frac{1}{z + \Delta z}\left[\left(z + \frac{\Delta z}{2}\right)\Delta\varepsilon_{eq} + (-\varepsilon_2^{eff} + \theta\varepsilon_1^{eff})\Delta z\right],
\end{aligned}
\tag{59}
$$

$$(\Delta \underline{\underline{a}}_1)_{OBJ} = \Delta \underline{\underline{a}}_1 + (\Delta \underline{\underline{a}}_1)_{GT} = \frac{2}{3}(1-p)\frac{\Delta \overline{\sigma}_1}{\Delta \varepsilon_1^{eff}}\Delta \varepsilon^p + (\Delta \underline{\underline{a}}_1)_T \Rightarrow$$

$$\Delta \underline{\underline{a}}_1 = \frac{2}{3}(1-p)\frac{\Delta \overline{\sigma}_1}{\Delta \varepsilon_1^{eff}}\Delta \varepsilon^p - (\Delta \underline{\underline{a}}_1)_{GT} + (\Delta \underline{\underline{a}}_1)_T, \tag{60}$$

$$\Delta(z\underline{\underline{a}}_2) = \frac{2}{3}(1-p)\left(z + \frac{\Delta z}{2}\right)\frac{\Delta \overline{\sigma}_2}{\Delta \varepsilon_2^{eff}}\Delta \varepsilon^p + \theta \underline{\underline{a}}_1 \Delta z - z(\Delta \underline{\underline{a}}_2)_{GT} + z(\Delta \underline{\underline{a}}_2)_T. \tag{61}$$

The quantities $\Delta \overline{\sigma}_1 / \Delta \varepsilon_1^{eff}$ and $\Delta \overline{\sigma}_2 / \Delta \varepsilon_2^{eff}$ intervening in the evolution equations of the parameters of the kinematic hardening are here the secant of strain hardening defined by:

$$\frac{\Delta \overline{\sigma}_i}{\Delta \varepsilon_i^{eff}} = \frac{1}{\Delta \varepsilon_i^{eff}}\left[\overline{\sigma}_i(\varepsilon_i^{eff} + \Delta \varepsilon_i^{eff}, T + \Delta T) - \overline{\sigma}_i(\varepsilon_i^{eff}, T + \Delta T)\right]. \tag{62}$$

This choice rather than that of the slopes of work hardening, as previously, is justified by compatibility with the resolution which follows, which will naturally make use again of the secants, this time for the isotropic part of the work hardening, via the exact respect of the criterion at the time $t + \Delta t$. Note also that equation (61) will be used in the given form, and not in the form of an expression of $\Delta \underline{\underline{a}}_2$ which will be less convenient here.

Now let us solve these equations by adopting $\Delta \varepsilon_{eq}$ as a key unknown. Proceeding as before from equations (54) and (57), we obtain

$$\underline{\underline{s}} + \Delta \underline{\underline{s}} = \underline{\underline{s}} + 2\mu \Delta \underline{\underline{e}} - (\Delta \underline{\underline{s}})_{GT} + (\Delta \underline{\underline{s}})_T - 2\mu \Delta \varepsilon^p,$$

which, by assuming as previously

$$(\underline{\underline{s}} + \Delta \underline{\underline{s}})^{el} = \underline{\underline{s}} + 2\mu \Delta \underline{\underline{e}} - (\Delta \underline{\underline{s}})_{GT} + (\Delta \underline{\underline{s}})_T \tag{63}$$

and using equation (56), is equivalent to

$$\underline{\underline{s}} + \Delta \underline{\underline{s}} = (\underline{\underline{s}} + \Delta \underline{\underline{s}})^{el} - 3\mu \frac{\Delta \varepsilon_{eq}}{F(\underline{\underline{s}} + \Delta \underline{\underline{s}} - \underline{\underline{a}} - \Delta \underline{\underline{a}})}(\underline{\underline{s}} + \Delta \underline{\underline{s}} - \underline{\underline{a}} - \Delta \underline{\underline{a}}).$$

By adding $-\underline{\underline{a}} - \Delta \underline{\underline{a}}$ to the two sides of the equations, and by writing $\underline{\underline{a}} + \Delta \underline{\underline{a}}$ in the form

$$\underline{\underline{a}} + \Delta \underline{\underline{a}} = (1 - z - \Delta z)(\underline{\underline{a}}_1 + \Delta \underline{\underline{a}}_1) + z\underline{\underline{a}}_2 + \Delta(z\underline{\underline{a}}_2)$$

and using equations (60) and (61), we get

$$
\begin{aligned}
\underline{\underline{s}} + \Delta \underline{\underline{s}} - \underline{\underline{a}} - \Delta \underline{\underline{a}} &= (\underline{\underline{s}} + \Delta \underline{\underline{s}})^{el} - 3\mu \frac{\Delta \varepsilon_{eq}}{F(\underline{\underline{s}} + \Delta \underline{\underline{s}} - \underline{\underline{a}} - \Delta \underline{\underline{a}})}(\underline{\underline{s}} + \Delta \underline{\underline{s}} - \underline{\underline{a}} - \Delta \underline{\underline{a}}) \\
&\quad - (1 - z - \Delta z)(\underline{\underline{a}}_1 + \Delta \underline{\underline{a}}_1) - z\underline{\underline{a}}_2 - \Delta(z\underline{\underline{a}}_2) \\
&= (\underline{\underline{s}} + \Delta \underline{\underline{s}})^{el} - (1 - z - \Delta z)\left[\underline{\underline{a}}_1 - (\Delta \underline{\underline{a}}_1)_{GT} + (\Delta \underline{\underline{a}}_1)_T\right] - z\underline{\underline{a}}_2 \\
&\quad - 3\mu \frac{\Delta \varepsilon_{eq}}{F(\underline{\underline{s}} + \Delta \underline{\underline{s}} - \underline{\underline{a}} - \Delta \underline{\underline{a}})}(\underline{\underline{s}} + \Delta \underline{\underline{s}} - \underline{\underline{a}} - \Delta \underline{\underline{a}}) \\
&\quad - (1 - z - \Delta z)\frac{2}{3}(1 - p)\frac{\Delta \overline{\sigma}_1}{\Delta \varepsilon_1^{eff}} \cdot \frac{3}{2}\frac{\Delta \varepsilon_{eq}}{F(\underline{\underline{s}} + \Delta \underline{\underline{s}} - \underline{\underline{a}} - \Delta \underline{\underline{a}})}(\underline{\underline{s}} + \Delta \underline{\underline{s}} - \underline{\underline{a}} - \Delta \underline{\underline{a}}) \\
&\quad - \frac{2}{3}(1 - p)\left(z + \frac{\Delta z}{2}\right)\frac{\Delta \overline{\sigma}_2}{\Delta \varepsilon_2^{eff}} \cdot \frac{3}{2}\frac{\Delta \varepsilon_{eq}}{F(\underline{\underline{s}} + \Delta \underline{\underline{s}} - \underline{\underline{a}} - \Delta \underline{\underline{a}})}(\underline{\underline{s}} + \Delta \underline{\underline{s}} - \underline{\underline{a}} - \Delta \underline{\underline{a}}) \\
&\quad - \theta \underline{\underline{a}}_1 \Delta z + z(\Delta \underline{\underline{a}}_2)_{GT} - z(\Delta \underline{\underline{a}}_2)_T.
\end{aligned}
$$

By using

$$
\begin{aligned}
\underline{\underline{s}}^* &\equiv (\underline{\underline{s}} + \Delta\underline{\underline{s}})^{el} - (1 - z - \Delta z)\left[\underline{\underline{a}}_1 - (\Delta\underline{\underline{a}}_1)_{GT} + (\Delta\underline{\underline{a}}_1)_T\right] \\
&\quad - z\underline{\underline{a}}_2 - \theta\underline{\underline{a}}_1 \Delta z + z(\Delta\underline{\underline{a}}_2)_{GT} - z(\Delta\underline{\underline{a}}_2)_T
\end{aligned}
\tag{64}
$$

(note that this definition is not the same as that of equation (39), in the case where the stress limit is not reached), and

$$
\widetilde{H} \equiv (1 - z - \Delta z)(1 - p)\frac{\Delta\overline{\sigma}_1}{\Delta\varepsilon_1^{eff}} + \left(z + \frac{\Delta z}{2}\right)(1 - p)\frac{\Delta\overline{\sigma}_2}{\Delta\varepsilon_2^{eff}}
\tag{65}
$$

this can be written as:

$$
\left[1 + \frac{(\widetilde{H} + 3\mu)\,\Delta\varepsilon_{eq}}{F(\underline{\underline{s}} + \Delta\underline{\underline{s}} - \underline{\underline{a}} - \Delta\underline{\underline{a}})}\right](\underline{\underline{s}} + \Delta\underline{\underline{s}} - \underline{\underline{a}} - \Delta\underline{\underline{a}}) = \underline{\underline{s}}^*.
\tag{66}
$$

Before going any further, let us give a simple and more meaningful expression of $\underline{\underline{s}}^*$. Let us denote $\underline{\underline{a}}_1 + (\Delta\underline{\underline{a}}_1)_{GT,T}$ and $\underline{\underline{a}}_2 + (\Delta\underline{\underline{a}}_2)_{GT,z,T}$ the values of $\underline{\underline{a}}_1$ and $\underline{\underline{a}}_2$ obtained by taking into account, in the variation $\Delta\underline{\underline{a}}_1$ and $\Delta\underline{\underline{a}}_2$, only the terms due to large transformations and variations of $z$ and $T$ (i.e., omitting the term proportional to $\Delta\underline{\underline{\varepsilon}}^p$). We have, by equations (60) and (61):

$$
\underline{\underline{a}}_1 + (\Delta\underline{\underline{a}}_1)_{GT,T} = \underline{\underline{a}}_1 - (\Delta\underline{\underline{a}}_1)_{GT} + (\Delta\underline{\underline{a}}_1)_T,
$$

$$
\begin{aligned}
(z + \Delta z)\lfloor\underline{\underline{a}}_2 + (\Delta\underline{\underline{a}}_2)_{GT,z,T}\rfloor - z\underline{\underline{a}}_2 &= \theta\underline{\underline{a}}_1 \Delta z - z(\Delta\underline{\underline{a}}_2)_{GT} + z(\Delta\underline{\underline{a}}_2)_T \\
\Rightarrow (z + \Delta z)\lfloor\underline{\underline{a}}_2 + (\Delta\underline{\underline{a}}_2)_{GT,z,T}\rfloor &= z\underline{\underline{a}}_2 + \theta\underline{\underline{a}}_1 \Delta z - z(\Delta\underline{\underline{a}}_2)_{GT} + z(\Delta\underline{\underline{a}}_2)_T.
\end{aligned}
$$

From these two expressions and equation (64), we can deduce that

$$
\begin{aligned}
\underline{\underline{s}}^* = (\underline{\underline{s}} + \Delta\underline{\underline{s}})^{el} - (1 - z - \Delta z)\lfloor\underline{\underline{a}}_1 + (\Delta\underline{\underline{a}}_1)_{GT,z,T}\rfloor - \\
(z + \Delta z)\lfloor\underline{\underline{a}}_2 + (\Delta\underline{\underline{a}}_2)_{GT,z,T}\rfloor.
\end{aligned}
\tag{67}
$$

This expression allows an easy calculation of $\underline{\underline{s}}^*$, having previously carried out the pre-corrections of $\underline{\underline{a}}_1$ and $\underline{\underline{a}}_2$ due to large transformations and variations of $z$ and $T$. Equation (66) implies that the (unknown) tensor $\underline{\underline{s}} + \Delta\underline{\underline{s}} - \underline{\underline{a}} - \Delta\underline{\underline{a}}$ is positively collinear with the (known) tensor, $\underline{\underline{s}}^*$, thereby

$$
\underline{\underline{s}} + \Delta\underline{\underline{s}} - \underline{\underline{a}} - \Delta\underline{\underline{a}} = \frac{F(\underline{\underline{s}} + \Delta\underline{\underline{s}} - \underline{\underline{a}} - \Delta\underline{\underline{a}})}{F(\underline{\underline{s}}^*)}\underline{\underline{s}}^*.
\tag{68}
$$

In addition, we obtain by taking the von Mises function of the two sides of equation (66):

$$
F(\underline{\underline{s}} + \Delta\underline{\underline{s}} - \underline{\underline{a}} - \Delta\underline{\underline{a}}) + (\widetilde{H} + 3\mu)\Delta\varepsilon_{eq} = F(\underline{\underline{s}}^*).
\tag{69}
$$

The equation (55) gives, by expliciting the yield limit thanks to equation (6):

$$
\begin{aligned}
F(\underline{\underline{s}} + \Delta\underline{\underline{s}} - \underline{\underline{a}} - \Delta\underline{\underline{a}}) &= [1 - f(z + \Delta z)]\,\sigma_1^Y(\varepsilon_1^{eff} + \Delta\varepsilon_1^{eff}, T + \Delta T)\\
&\quad + f(z + \Delta z)\sigma_2^Y(\varepsilon_2^{eff} + \Delta\varepsilon_2^{eff}, T + \Delta T)\\
&= [1 - f(z + \Delta z)]\left[\sigma_1^Y(\varepsilon_1^{eff}, T + \Delta T) + p\frac{\Delta\overline{\sigma}_1}{\Delta\varepsilon_1^{eff}}\Delta\varepsilon_1^{eff}\right]\\
&\quad + f(z + \Delta z)\left[\sigma_2^Y(\varepsilon_1^{eff}, T + \Delta T) + p\frac{\Delta\overline{\sigma}_2}{\Delta\varepsilon_2^{eff}}\Delta\varepsilon_2^{eff}\right]\\
&= \sigma^Y(\varepsilon_1^{eff}, \varepsilon_2^{eff}, z + \Delta z, T + \Delta T)\\
&\quad + [1 - f(z + \Delta z)]p\frac{\Delta\overline{\sigma}_1}{\Delta\varepsilon_1^{eff}}\Delta\varepsilon_1^{eff} + f(z + \Delta z)p\frac{\Delta\overline{\sigma}_2}{\Delta\varepsilon_2^{eff}}\Delta\varepsilon_2^{eff},
\end{aligned}
$$

which gives, by reporting in equation (69):

$$
\begin{aligned}
&\sigma^Y(\varepsilon_1^{eff}, \varepsilon_2^{eff}, z + \Delta z, T + \Delta T) + [1 - f(z + \Delta z)]p\frac{\Delta\overline{\sigma}_1}{\Delta\varepsilon_1^{eff}}\Delta\varepsilon_1^{eff}\\
&\quad + f(z + \Delta z)p\frac{\Delta\overline{\sigma}_2}{\Delta\varepsilon_2^{eff}}\Delta\varepsilon_2^{eff} + (\widetilde{H} + 3\mu)\Delta\varepsilon_{eq} = F(\underline{\underline{s}}^*).
\end{aligned}
$$

This equation can be written as, according to equations (58) and (59):

$$
(H + 3\mu)\Delta\varepsilon_{eq} = \Delta, \tag{70}
$$

$$
\begin{aligned}
H \equiv \widetilde{H} &+ [1 - f(z + \Delta z)]p\frac{\Delta\overline{\sigma}_1}{\Delta\varepsilon_1^{eff}} + f(z + \Delta z)\frac{z + \Delta z/2}{z + \Delta z}p\frac{\Delta\overline{\sigma}_2}{\Delta\varepsilon_2^{eff}}\\
&= (1 - z - \Delta z)(1 - p)\frac{\Delta\overline{\sigma}_1}{\Delta\varepsilon_1^{eff}} + \left(z + \frac{\Delta z}{2}\right)(1 - p)\frac{\Delta\overline{\sigma}_2}{\Delta\varepsilon_2^{eff}}\\
&\quad + [1 - f(z + \Delta z)]p\frac{\Delta\overline{\sigma}_1}{\Delta\varepsilon_1^{eff}} + f(z + \Delta z)\frac{z + \Delta z/2}{z + \Delta z}p\frac{\Delta\overline{\sigma}_2}{\Delta\varepsilon_2^{eff}},
\end{aligned} \tag{71}
$$

$$
\begin{aligned}
\Delta \equiv F(\underline{\underline{s}}^*) &- \sigma_1^Y(\varepsilon_1^{eff} + \Delta\varepsilon_1^{eff}, T + \Delta T) + f(z + \Delta z)p\frac{\Delta\overline{\sigma}_2}{\Delta\varepsilon_2^{eff}}\frac{\Delta z}{z + \Delta z}\times\\
&(\varepsilon_2^{eff} - \theta\varepsilon_1^{eff}).
\end{aligned} \tag{72}
$$

Equation (70) relates to the only unknown $\Delta\varepsilon_{eq}$, the strain hardening secants depends on the $\varepsilon_1^{eff}$ which are expressed as a function of $\Delta\varepsilon_{eq}$, thanks to the equations (58) and (59). It can be solved, for example, by the method of the fixed point. The quantity $F(\underline{\underline{s}} + \Delta\underline{\underline{s}} - \underline{\underline{a}} - \Delta\underline{\underline{a}})$ is then deduced from equation (55) and then the tensor $\underline{\underline{s}} + \Delta\underline{\underline{s}} - \underline{\underline{a}} - \Delta\underline{\underline{a}}$ is deduced from equation (68). Finally, we calculate $\Delta\underline{\underline{\varepsilon}}^p$ thanks to equation (56), then $\underline{\underline{a}}_1$ and $\underline{\underline{a}}_2$ thanks to equations (60) and (61).

## 5.3. Particular case: isotropic strain hardening with the yield limit not reached

If the yield limit is not reached, the expression of equation (29) proposed for $(\Delta\sigma_1^{eq})_s$ is applicable whatever the type of the work hardening. However, for a pure isotropic work hardening, $p \equiv 1$ is equivalent to the expression (10) of $(\dot{\sigma}_1^{eq})_s$ and can also be written equivalently (with $(\underline{\underline{a}}_1 \equiv \underline{\underline{0}})$) as:

$$
(\dot{\sigma}_1^{eq})_s \equiv \frac{3}{2\sigma^{eq}}\underline{\underline{s}} : \overset{\triangledown}{\underline{\underline{s}}} = \dot{\sigma}_{eq} \quad , \quad \sigma_{eq} \equiv \left(\frac{3}{2}\underline{\underline{s}} : \underline{\underline{s}}\right)^{\frac{1}{2}}.
$$

We can then assume that a simple expression for $(\Delta\sigma_1^{eq})_s$, than equation (29)

$$(\Delta\sigma_1^{eq})_s \equiv Y \equiv \Delta\sigma_{eq} = F(\underline{s} + \Delta\underline{s}) - F(s) \equiv X - F(\underline{s}). \tag{27''}$$

This simplification is adopted in several finite element codes. It is necessary to take again the elements of the numerization exposed in Section 4.1 in the case of the purely isotropic work hardening where the yield stress is not reached.

The equation (42) being obtained without using the expression (29) of $(\Delta\sigma_1^{eq})_s \equiv Y \equiv \Delta\sigma_{eq}$ is valid here also; it can be written as, with $\underline{a}_1 \equiv \underline{0}, \Delta\underline{a}_1 \equiv \underline{0}, p \equiv 1$ (thus, $H = 0$ from equation (40)):

$$\left[ 1 + \mu(A + BY)\left( 1 + \frac{F(\underline{s})}{X} \right) \right](\underline{s} + \Delta\underline{s}) = \underline{s}^*.$$

$\underline{s}^*$ is always given by equation (39), with $\underline{a}_1 \equiv \underline{0}, (\Delta\underline{a}_1)_T \equiv \underline{0}$

$$X + \mu(A + BY)(X + F(\underline{s})) = X + \mu[A + B(X - F(\underline{s}))](X + F(\underline{s})) = F(\underline{s}^*).$$

The equation (43) then applied always, with $\underline{a}_1 \equiv \underline{0}, \Delta\underline{a}_1 \equiv \underline{0}$. In addition, taking into account the function of von Mises of the two sides of equation (42") and taking into account equation (29"), we obtain:

$$L''X^2 + M''X + N'' = 0, \tag{44''}$$

which gives by re-ordering the terms

$$L'' + \mu B, \tag{45''}$$

$$M'' = 1 + \mu A, \tag{46''}$$

$$N'' = \mu A F(\underline{s}) - \mu B F^2(\underline{s}) - F(\underline{s}^*). \tag{47''}$$

As in the usual case, this formulation does not necessarily ensure that there exists a positive real solution $X$. If this is not the case, we can adopt a completely implicit algorithm (replacement of equations (25) and (26) by equations (25') and (26')). This leads to replacing $F(\underline{s})$ by $F(\underline{s} + \Delta\underline{s} \equiv X$ in equation (42'), which becomes:

$$[1 + 2\mu(A + BY)](\underline{s} + \Delta\underline{s}) = \underline{s}^*. \tag{40'''}$$

By taking the von Mises function of the two sides of the previous equations and taking into account equation (29"), we then obtain

$$X + 2\mu X[A + B(X - F(\underline{s}))] = F(\underline{s}^*),$$

which is equivalent to

$$L'''X^2 + M'''X + N''' = 0, \tag{44'''}$$

$$L''' + 2\mu B, \tag{45'''}$$

$$M''' = 1 + 2\mu(A - BF(\underline{s})), \tag{46'''}$$

$$N''' = -F(\underline{s}^*). \tag{47'''}$$

Since $L''' > 0$ and $N''' > 0$, the existence of this unique positive solution is therefore guaranteed.

### 5.4. Numerical treatment of the delocalization

The procedure employs an array $\mathcal{A}(\text{I, J})$, where the first index ranges from 1 to 6 and the second index spans the total number of Gauss points affected by the delocalization, signifying each specific Gauss point. The significance of the quantities $\mathcal{A}(\text{I, J})$ is profound:

- $\mathcal{A}(1,\ \text{J}), \mathcal{A}(2,\text{J}), \mathcal{A}(3,\text{J})$: Precise coordinates of Gaussian point J;
- $\mathcal{A}(4,\ \text{J})$: Immediate local effective plastic strain increment (between times $t$ and $t + \Delta t$) at Gaussian point J;
- $\mathcal{A}(5,\text{J})$: Authentic increment (post convolution) of effective plastic strain at Gaussian point J;
- $\mathcal{A}(6,\text{J})$: Weight of Gauss point (for integration).

The computational process is resolute as follows: at every iteration and for each Gauss point, a meticulously crafted program meticulously calculates the coordinates and weight of the Gauss point, meticulously storing them in $\mathcal{A}(1 - 3, \text{J})$ and $\mathcal{A}(6, \text{J})$. Furthermore, it invokes a meticulously engineered sub-program that assesses the local effective plastic strain increment; this valuable information is meticulously recorded in $\mathcal{A}(4,\ \text{J})$. Upon achieving convergence on the nodal imbalances, another meticulously designed program is executed, which, through a double loop on the Gauss points, meticulously executes the convolution operation. The resulting effective plastic strain increment at point $J$, meticulously preserved in $\mathcal{A}(5,\ \text{J})$, is conveyed to a meticulously crafted program responsible for the ultimate task of calculating and meticulously preserving the effective plastic strain at time $t$ and $t + \Delta t$. The procedure is executed twice for both nonlocal effective plastic strain variables.

## 6. Numerical results/comparison with experiments/discussion

The constitutive model presented in the first section is essentially based on von Mises model; this model is a widely used constitutive model in solid mechanics and has been extensively studied and validated in the literature. Previous research has shown that the von Mises model typically exhibits known behavior with respect to mesh size variations. Specifically:

- The behavior of the von Mises model with respect to mesh size variations is well understood. Studies have demonstrated that the model's predictions converge to a stable solution as the mesh size is refined. Sensitivity analyses have shown that the model's output is relatively insensitive to changes in mesh size within a certain range.
- The von Mises model has undergone thorough validation against experimental data or benchmark simulations. It has been shown to provide accurate predictions within an acceptable range of mesh sizes. Validation efforts have included comparisons with experimental measurements, analytical solutions, and other well-established models or industry standards.

Given the known behavior and extensive validation of the von Mises model, conducting additional mesh size dependency checks may be redundant. Instead, we shall focus on ensuring that the simulation results accurately mirror the experimental data.

The algorithm described above is implemented in Systus to evaluate the model described above. The numerical modeling pertains to a martensitic transformation of A508 steel, as first demonstration of the robustness of the algorithm. The transformation deformation is solely induced by thermal deformation (the expansion of the daughter phase) without including any deviatoric component (neglecting shape change). The results of this modeling provide a better understanding of the behavior of A508 steel during its martensitic transformation. This data is crucial for optimizing heat treatment processes and designing A508 steel components for specific applications, such as nuclear construction. The thermo-mechanical properties assumed for the two phases are as follows:

The transformation of an element occurs through a change in its thermo-elastic properties from phase $\gamma$ to phase $\alpha$. During this transformation, a uni-axial stress with a constant amplitude of approximately 1/3 of the yield strength of the weaker phase is applied to the material. This study will demonstrate that the first type of transformation (diffusive progression of the elements to be transformed) provides a better agreement with the theoretical predictions of the author's analytical model.

We will numerically investigate transformation plasticity, focusing on Greenwood and Johnson's mechanism. In this study, a finite element mesh will undergo external loading, with sequential element transformations by
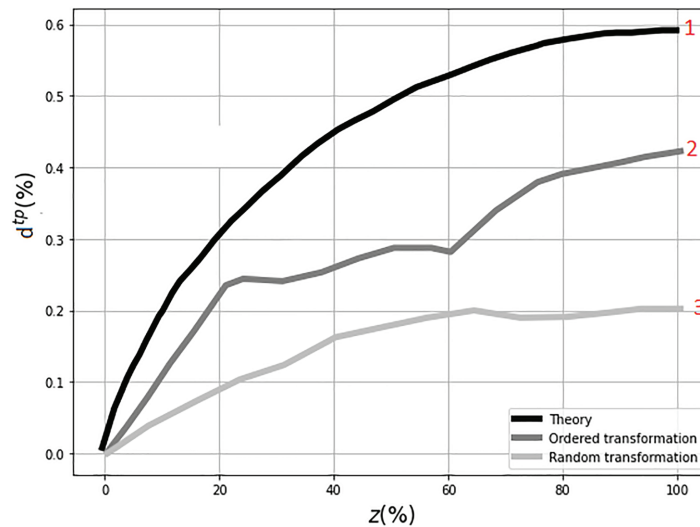
**Figure 2.** Transformation plastic strain in a $5 \times 5 \times 5$ cube for a stress equals to 50 MPa: (1) theory; (2) ordered transformation, $\Sigma_{11}$ = 50 MPa; and (3) random transformation.

changing their thermal strain and yield stress from those of the $\gamma$ phase to those of the $\alpha$ phase. The transformation strain will consist only of the difference of thermal strain between the phases and will not include any deviatoric part (change of shape).

The transformation studied is the martensitic transformation of the A.508 cl. 3 steel. The temperature dependence of the thermo-mechanical characteristics is disregarded. These characteristics are provided in the document 8 appended to this paper. The characteristic length scales involved in the nonlocality added to the model are $l_1 = l_2 = 200 \ \mu$m, above the finite element discretization size. By setting both length scales equal, the model assumes some "isotropy" in the nonlocal effects, meaning that the influence of material properties or deformations extends uniformly in all directions around a given point. This assumption simplifies the modeling process and allows for a more straightforward implementation of nonlocality in the simulation framework.

The chosen representative elementary volume (REV) for modeling transformation plasticity is a regular $5 \times 5 \times 5$ mesh cube. Note that a similar mesh is used by Leblond et al. [11, 12], but their model did not account for nonlocal effects to address the post-bifurcation mesh size effects. Also, the phases exhibit perfectly plastic behavior (without hardening). Two types of transformations are studied:

1.    Elements are transformed in a specific order, from the center of the REV to its boundaries.
2.    Elements are transformed in a random order within the REV.

The transformation of an element occurs through a change in its thermo-elastic properties from phase $\gamma$ to phase $\alpha$. During this transformation, a uni-axial stress with a constant amplitude of about 1/3 of the yield strength of the weakest phase is applied to the REV.

This study demonstrates that the first type of transformation (diffusive progression of the elements to be transformed) provides a better agreement with the theoretical predictions of the author's analytical model.

Figure 2 illustrates the plastic strain resulting from transformation in a $5 \times 5 \times 5$ cube under an applied stress of 50 MPa, capturing both ordered and random transformations. This visual depiction serves as a comprehensive snapshot of the material's response to the specified stress conditions, offering a comparative analysis between the two transformation scenarios.

Analyzing the curve associated with an ordered transformation originating from the center substantiates this interpretation. In the initial stages of the transformation, only interior elements undergo the process, resulting in a curve with a slope twice as steep as the preceding one. During this phase, the computed results align well with theoretical expectations. However, when surface elements come into play in the transformation process, there is a sudden and pronounced decrease in the slope, leading to a diminished agreement between computational outcomes and theoretical predictions.

As the transformation unfolds, the surface elements exhibit a distinctive response characterized by a more facile outward expansion in contrast to their inward progression. This asymmetry in the transformation dynamics stems from the augmented volume experienced by the surface elements during the process. Consequently,
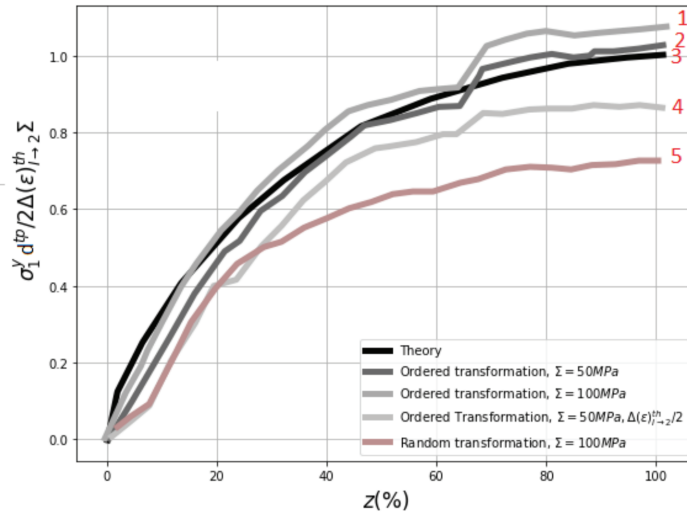
**Figure 3.** Normalized transformation plastic strain in a $10 \times 10 \times 10$ cube for lower stresses: (1) theory; (2) ordered transformation, $\Sigma_{11} = 50$ MPa; (3) ordered transformation, $\Sigma_{11} = 100$ MPa; (4) same as in (2) except that difference of thermal strain between the two phases is divided by 2; and (5) random transformation, $\Sigma_{11} = 100$ MPa.

the plastic strains induced in the austenitic phase manifest with diminished prominence when compared to their counterparts within the cube's interior. This nuanced phenomenon intricately underpins the underestimation of the Greenwood–Johnson effect, attributing this discrepancy to the ostensibly inconsequential yet influential presence of surface elements.

Extending our scrutiny to an ordered transformation originating from the center, a compelling narrative emerges. In the initial stages, wherein only interior elements partake in the transformation, the resultant curve exhibits a slope twice as steep as its random transformation counterpart. This phase aligns seamlessly with theoretical expectations, portraying a harmonious relationship between computation and theory. However, the plot takes a fascinating turn when surface elements become integral to the transformation process.

Upon the involvement of surface elements, a sudden and pronounced decrease in slope unfolds, ushering in a phase marked by a notable misalignment between computational outcomes and theoretical predictions. This inflection point underscores the critical role played by surface elements in shaping the transformation dynamics, offering a deeper understanding of the complex interplay between internal and surface influences on the observed mechanical behavior. In essence, the juxtaposition of random and ordered transformations unravels a rich tapestry of insights, shedding light on the multifaceted nature of material transformations and the consequential impact of seemingly peripheral factors.

Figure 3, serving as the counterpart to Figure 2, replicates the experimental setup, albeit with a diminished mesh size, featuring a cube measuring $10 \times 10 \times 10$ units. A notable adjustment in the applied stresses has been introduced, elevating them from 50 MPa to a more substantial 100 MPa. Furthermore, both random and ordered modes of "normalized" transformation were deliberately incorporated into the experimental conditions.

In contrast to its predecessor, Figure 3 encapsulates the same experimental essence but with a finer spatial resolution achieved through a reduced mesh size. The alteration in stress parameters, escalating from 50 to 100 MPa, introduces a heightened mechanical loading scenario, accentuating the influence of external forces on the transformation phenomena. This augmentation in stress levels serves to amplify the mechanical responses within the $10 \times 10 \times 10$ cube, providing a nuanced perspective on the material's behavior under varying stress conditions.

The intentional inclusion of both random and ordered transformations in this iteration broadens the scope of the investigation, allowing for a comprehensive analysis of the material's response to distinct transformation mechanisms. This deliberate diversification in transformation types enriches the experimental landscape, facilitating a more thorough exploration of the material's mechanical behavior and its sensitivity to different transformation pathways. The juxtaposition of these transformation modes within the refined experimental setup introduces a layer of complexity, offering a more nuanced understanding of the material's response to varying stress regimes.

It is noteworthy that both transformation orders now yield results that are mutually consistent and align with theoretical expectations. This observation indicates a significant reduction in the influence of surface elements, underscoring the enhanced congruence between the outcomes and theoretical predictions.

We can envisage to investigate the case of very large applied stresses, surpassing the critical yield strength ($\Sigma_y$) threshold of 145 MPa. This represents a significant departure from conventional stress levels, introducing a novel challenge in understanding material behavior under extreme conditions.

At such elevated stress levels, it becomes evident that traditional experimental methods and existing theoretical frameworks may no longer suffice to comprehensively capture the intricate nuances of material response. The absence of empirical data and established theories for stress magnitudes beyond $\Sigma_y = 145$ MPa underscores the need for alternative approaches to model transformation plasticity.

In this context, numerical simulations emerge as indispensable tools for bridging the knowledge gap. They play a pivotal role in not only compensating for the lack of experimental data but also in establishing a robust and realistic model for transformation plasticity under these unprecedented stress regimes. The reliance on numerical simulations becomes paramount as they offer a flexible and efficient means to explore and comprehend complex material behaviors that elude conventional experimental techniques.

In essence, our exploration of very large applied stresses necessitates a paradigm shift in our approach. The synergy between experimental insights, theoretical frameworks, and numerical simulations is key to advancing our understanding of transformation plasticity under these challenging conditions.

## 7. Comparative analysis across theories, empirical studies, and micro-mechanical simulations

Comparisons of the model predictions with experiments conducted on A533 steel transformation plasticity by Desalos [26] serve as another crucial benchmark for validating our numerical implementation. The insights gained from these comparisons add a significant layer of confidence to the reliability of our simulations. The physical constants employed in our numerical model for this case, characterizing the $\gamma$- and $\alpha$- phases of A533 steel, closely mirror those derived from the meticulous experimental investigations of Desalos [26] and Coret et al. [27, 28]. Notably, our material properties feature identical values for Young's modulus ($E = 182,000$ MPa) and Poisson's ratio ($\nu = 0.3$) across both phases, for the rest of the material constants used for the simulations with the A533 steel can be found in Desalos [26] and Coret et al. [27, 28].

Furthermore, our choice of yield stress parameters is well-founded, with $\Sigma_m = 145$ MPa assigned to the mother phase and $\Sigma_D = 950$ MPa to the daughter phase. This meticulous adherence to established values enhances the credibility of our numerical model. Additionally, we account for the relative change of specific volume from the mother to the daughter phase. These constants, consistently applied and well documented, collectively contribute to the robustness of our numerical model, thereby fortifying the reliability and validity of our research findings.

In the examined cases for comparative analysis, the RVE is a spherical volume made of an elastic-plastic material which experiences some external loading via homogeneous boundary stress (HBStress) or homogeneous boundary strain (HBStrain) conditions to ensure robustness. The primary goal is to strengthen the theoretical analysis, with a specific emphasis on HBStress conditions, while rigorously examining the influence of boundary conditions. The consequential plastic strain transformation along the loading direction is identified as $d^{pt}(z)$, capturing the intricate evolution of the material under this specific stress condition. (Any other components are omitted, either being zero or directly correlated to $d^{pt}(z)$ owing to considerations of incompressibility.)

In Figure 4, the progression of the transformation plastic strain is depicted, illustrating the dynamic evolution as the transformation unfolds. This evolution is characterized by the ratio $d^{pt}(z)/d^{pt}(1)$, a metric that ascends from 0 to 1. The dependence on the volume fraction $z$ of the daughter phase is evident in the plot. The graph not only captures this transformational journey but also highlights the significant variations in the ratio across different values of $z$.

The depicted data is a comparative analysis involving the predictions of three distinct formulas. First, the original formula (19) proposed by Leblond et al. [12] is represented. Second, an allegedly improved variant (20) of the original formula is included in the comparison. Finally, Desalos [26] introduces a phenomenological formula, $d^{pt}(z)/d^{pt}(1) \approx z(2 - z)$, which he found to be universally applicable to all his experimental results for the A533 steel, regardless of the stress applied. The juxtaposition of these formulas provides a comprehensive
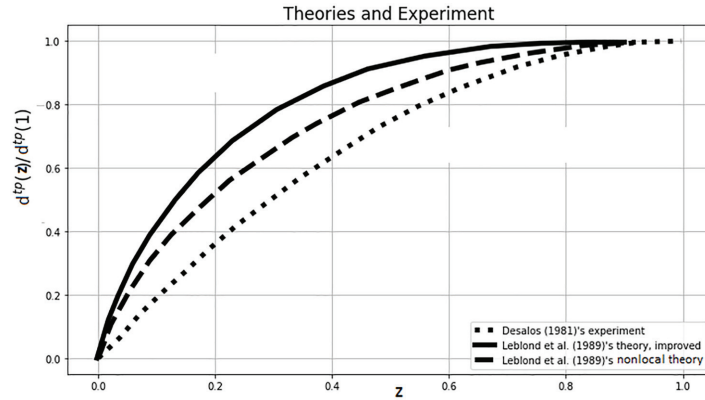
**Figure 4.** Comparison of the evolution of the transformation plastic strain: theories and experiments.
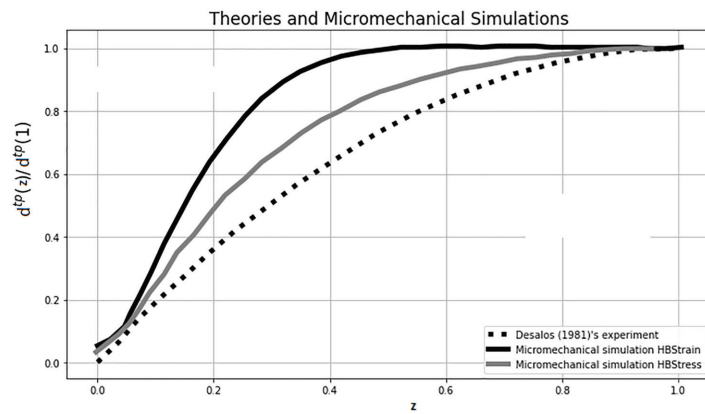


**Figure 5.** Evolution of transformation plastic strain: a comparative analysis between experiments and micro-mechanical simulations.

view of their predictive capabilities and sheds light on their performance across the spectrum of volume fractions and stress values.

All theoretical curves, with the exception of the one corresponding to the purportedly enhanced variant of Leblond et al.'s [12] original formula, equation (11), offer sensible depictions of Desalos' [26] experimental findings. Nevertheless, across all scenarios, the projected escalation in transformation plastic strain proves somewhat accelerated during the initial half of the transformation process.

In Figure 5, a comparative analysis is presented, juxtaposing the outcomes derived from micro-mechanical simulations conducted under both HBStress and HBStrain conditions. Notably, these simulations were executed under a low stress condition, precisely $\Sigma = 20$ MPa. It is imperative to highlight that, for contextual reference, the curve representing Desalos' [26] heuristic formula, previously discussed and applicable across the entire spectrum of stresses he considered, is once again included. This additional visual cue serves as a point of reference, facilitating a comprehensive understanding of the observed results and their alignment with established heuristic models.

A substantial disparity exists in the numerical outcomes derived under HBStress and HBStrain conditions, underscoring the profound impact of boundary conditions. This stark contrast serves to highlight the inherent limitations associated with an approach centered on a simplistic and diminutive RVE, exemplified by a spherical volume of the mother phase housing a solitary growing core of the daughter phase. This discrepancy not only underscores the sensitivity of the results to the chosen boundary conditions but also provides tangible evidence of the inadequacies inherent in employing such a rudimentary RVE model.

Next, we embark on an exploration of the "amplitude" of transformation plasticity, denoted by the value of the transformation plastic strain after the completion of the transformation process, $d^{tp}(1)$. In the illustrative Figure 6, this parameter unfolds its dependencies in response to the applied overall stress. Specifically, this juxtaposes diverse perspectives, offering a comprehensive comparison among Leblond et al.'s [12] original formula (11), and Desalos's [26] experimental findings for the A533 steel.
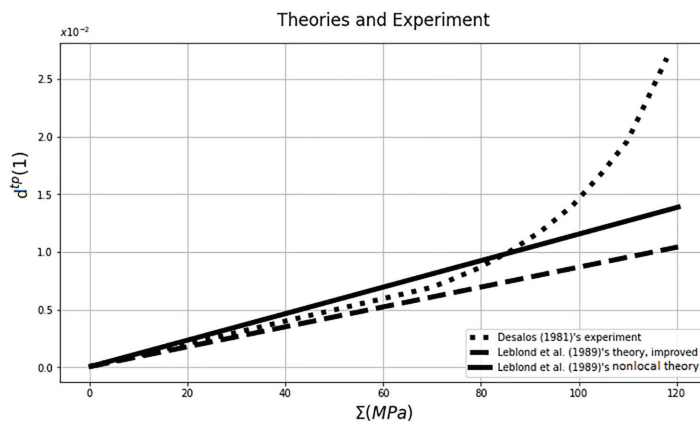
**Figure 6.** A comparative analysis of plastic strains following full transformation: bridging the divide between theoretical projections and experiments.
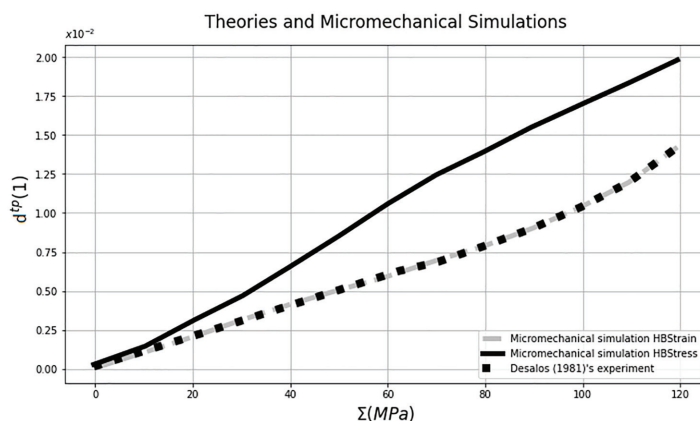


**Figure 7.** Comparative analysis of plastic strains following full transformation: experiments versus micro-mechanical simulations.

Desalos' [26] empirical findings, encapsulated in the heuristic formula $d_{pt}(1) = 10^{-4}\Sigma$ (with units in MPa), remarkably align with the predicted outcomes, substantiating the robustness and applicability of our general formula (11) in capturing the amplitude of transformation plasticity. This comparative analysis not only serves as a validation of existing models but also unveils the intricate relationship between theoretical predictions and experimental observations in the realm of transformation plasticity, providing a nuanced understanding of material behavior under varying stress conditions.

In Figure 7, a comprehensive comparison unfolds between the predictions derived from our overarching formula (11) and the outcomes gleaned from micro-mechanical simulations conducted under HBStress and HBStrain conditions. Notably, for reference, Desalos' [26] experimental results are once again presented, lending an additional layer of context and validation to the juxtaposition of our theoretical predictions with real-world observations.

The numerical outcomes derived under HBStress and HBStrain conditions exhibit a notable disparity, further highlighting the divergence in their respective influences. However, a noteworthy reversal of this trend is observed when considering the ratio $d^{pt}(z)/d^{pt}(1)$. In contrast to the previous scenario, results associated with HBStrain conditions surpass those under HBStress conditions in this context, with reference to Desalos' [26] experimental findings.

It becomes apparent that under HBStress conditions, there is a conspicuous tendency for an overestimation of the amplitude of transformation plasticity. This discrepancy underscores the critical role of the chosen stress conditions in influencing the accuracy of predictions, particularly in comparison to experimental benchmarks. The inversion of performance between HBStress and HBStrain conditions underscores the nuanced interplay of factors and the need for a comprehensive understanding of the material response under varying conditions.

## 8. Conclusion

In conclusion, our research underscores the profound significance of transformation plasticity in shaping the outcomes of crucial industrial processes, particularly those involving solid–solid phase transitions such as welding and quenching. The ability to accurately simulate and predict the behavior of materials undergoing such transformations is imperative for ensuring the integrity and efficiency of these processes. Our study highlights the intricate interplay of thermal, metallurgical, and mechanical effects that govern the evolution of material properties during phase transitions.

While Leblond and co-workers' model provided a foundational framework for understanding transformation plasticity, our work demonstrates the critical need for refinement, particularly in addressing the complexities of mixed isotropic/kinematic hardening. By augmenting this model with characteristic length scales and nonlocal variables, we have achieved a more comprehensive understanding of the underlying plastic deformation mechanisms operating in both phases of the material.

Our methodology involved not only theoretical enhancements but also practical implementation through numerical simulations within a finite element analysis framework. By applying our refined model to real-world scenarios involving A.508cl. and A533 steels, we have validated its efficacy in capturing the intricate nuances of phase transformation phenomena. The robustness and efficiency demonstrated by our model in predicting these behaviors underscore its potential to significantly enhance industrial practices.

In essence, our findings represent a significant step forward in the quest for high-fidelity predictive models of transformation plasticity. By shedding light on the underlying mechanisms and refining our ability to simulate and predict material behavior, our research offers tangible benefits to a wide range of industrial applications. From improving the performance and reliability of manufacturing processes to enabling the development of advanced materials with tailored properties, the implications of our work extend far beyond the confines of academic research. We believe that our study not only advances the state of the art in materials science and engineering but also holds promise for driving innovation and efficiency across diverse industrial sectors.

### ORCID iD

Koffi Enakoutsa https://orcid.org/0000-0002-1061-4511

## References

[1] Inoue, T, Nakano, M, Kubo, T, et al. High accuracy control of a proton synchrotron magnet power supply. *IFAC Proceedings Volumes* 1981; 14(2): 3137–3142.

[2] Inoue, T, and Wang, Z. Coupling between temperature, stress and metallic structures during phase transformation and the analysis of carburized quenching of a steel gear. In: Yagawa, G, and Atluri, S (eds) *Computational mechanics'86*. Cham: Springer, 1986, pp. 691–696.

[3] Fukumuto, M, Yoshizaki, M, Imataka, H, et al. Three-dimensional FEM analysis of helical gear subjected to the carburized quenching process. *Zairyo* 2001; 50(6): 598–605.

[4] Miyao, K, Wang, Z, and Inoue, T. Analysis of temperature, stress and metallic structure in carburized quenched gear considering transformation plasticity. *J Soc Mat Sci* 1986; 35(399): 1352–1357.

[5] Taleb, L, and Sidoroff, F. A micromechanical modeling of the Greenwood-Johnson mechanism in transformation induced plasticity. *Int J Plast* 2003; 19: 1821–1842.

[6] Greenwood, GW, and Johnson, R. The deformation of metals under small stresses during phase transformations. *Proc R Soc London Ser A* 1965; 283(1394): 403–422.

[7] Magee, CL, and Paxton, HW. Transformation kinetics, microplasticity and aging of martensite in Fe-31 Ni. Technical report, Carnegie Institute of Technology, Pittsburgh, PA, 1 September 1966.

[8] De Jong, M, and Rathenau, G. Mechanical properties of an iron-carbon alloy during allotropic transformation. *Acta Metall* 1961; 9(8): 714–720.

[9] Bhadeshia, H. The bainite transformation: unresolved issues. *Mater Sci Eng* 1999; 273–275: 58–66.

[10] Bhadeshia, H. Carbon-carbon interactions in iron. *J Mater Sci* 2004; 39: 3949–3955.

[11] Leblond, JB, Mottet, G, and Devaux, JC. A theoretical and numerical approach to the plastic behaviour of steels during phase transformations–I. Derivation of general relations. *J Mech Phys Solids* 1989; 34(4): 395–409.

[12] Leblond, JB, Mottet, G, and Devaux, JC. A theoretical and numerical approach to the plastic behaviour of steels during phase transformations–II. Study of classical plasticity for ideal-plastic phases. *J Mech Phys Solids* 1986; 34(4): 411–432.

[13] Leblond, JB, Perrin, G, and Devaux, J. Bifurcation effects in ductile metals with nonlocal damage. *J Appl Mech Trans ASME* 1994; 61: 236–242.

[14] Enakoutsa, K, Leblond, JB, and Perrin, G. Numerical implementation and assessment of a phenomenological nonlocal model of ductile rupture. *Comput Methods Appl Mech Eng* 2007; 196: 1946–1957.

[15] Enakoutsa, K. *Modéle non-locaux en rupture ductile des métaux*. PhD Thesis, Université Pierre et Marie Curie (Paris VI), Paris, 2007.

[16] Enakoutsa, K, and Leblond, JB. Numerical implementation and assessment of the GLPD micromorphic model of ductile rupture. *Eur J Mech A Solids* 2009; 28: 445–460.

[17] Ahad, F, Enakoutsa, K, Solanki, K, et al. Nonlocal modeling in high velocity impact failure of aluminum 6160-T6. *Int J Plast* 2013; 55: 108–132.

[18] Enakoutsa, K. Some new applications of the GLPD micromorphic model for ductile fracture. *Math Mech Solids* 2012; 19(3): 242–259.

[19] Enakoutsa, K, Solanki, K, Ahad, F, et al. Using damage delocalization to model localization phenomena in Bammann-Chiesa-Johnson metals. *J Eng Mater Technol* 2012; 134(4): 041014.

[20] Enakoutsa, K, Solanki, K, Ahad, F, et al. Damage smoothing effects in a delocalized rate sensitivity model for metals. *Theor Appl* 2012; 2(5): 051005.

[21] Enakoutsa, K. An analytic benchmark solution to the problem of a generalized plane strain hollow cylinder made of micromorphic plastic porous metal and subjected to axisymmetric loading conditions. *Math Mech Solids* 2015; 20(9): 1013–1025.

[22] Enakoutsa, K, and Li, Y. Mastering the art: proficient finite element implementation and robust evaluation of a strain-hardening porous ductile material crack growth prediction model at finite strain. *Appl Math Model* 2024; 132: 73–108.

[23] Enakoutsa, K. Analytical applications and effective properties of a second gradient isotropic elastic material model. *Z Angew Math Phys* 2015; 66: 1277–1293.

[24] Enakoutsa, K, and Bills, YL. Moving from theory to application: evaluating the numerical implementation of void shape effects and damage delocalization in the modeling of ductile fracture in porous plastic metals. *Math Mech Solids* 2024; 29: 1432–1456.

[25] Pijaudier-Cabot, G, and Bazant, ZP. Nonlocal damage theory. *J Eng Mech* 1987; 113: 1512–1533.

[26] Desalos, Y. Comportement mécanique et dilatométrique de l'austénite métastable de l'acier A533. Technical Report 95349401, IRSID, Institut de La Recherche de la Siderurgie, 1981.

[27] Coret, M, Calloch, S, and Cambescure, A. Experimental study of the phase transformation plasticity of 16MND5 low carbon steel under multiaxial loading. *Int J Plast* 2002; 18(12): 1707–1727.

[28] Coret, M, Calloch, S, and Cambescure, A. Experimental study of the phase transformation plasticity of 16MND5 low carbon steel induced by proportional and nonproportional biaxial loading paths. *Eur J Mech A Solids* 2004; 23(5): 823–842.

[29] Greenwood, GW, and Johnson, RH. The deformation of metals under small stresses during phase transformations. *Proc R Soc London Ser A* 1965; 283: 403–422.

[30] Leblond, JB. Simulation numérique du soudage-modélisation mathématique des transformations métallurgiques-état d'avancement des travaux. Technical report, Framatome Internal Report #TM/C DC/80.066, 1980.

# Appendix 1

## *The material properties for the A.508 cl. 3 steel*

The material properties for the A.508 cl. 3 steel include Young's modulus, thermal conductivity, Poisson ratio, yield limit, and hardening rate. These properties play crucial roles in determining the mechanical and thermal behavior of the steel alloy. These properties are summarized in Table 1 for each of the phases the steel is made of:

**Table 1.** The material properties for the A.508 cl. 3 steel, from Leblond et al. [11, 12].

|  | Phase $\alpha$ | Phase $\gamma$ |
| --- | --- | --- |
| Young's modulus (MPa) | 182,000 | 182,000 |
| Poisson ratio | 0.3 | 0.3 |
| Yield limit (MPa) | 950 | 145 |
| Hardening rate | 0 | 0 |
| Thermal deformation | 0 | 0.84% |

## The material properties for the A533 steel

The material properties for the A533 steel include Young's modulus, Poisson ratio, and yield limit. These properties play crucial roles in determining the mechanical properties of the steel alloy. These properties are summarized in Table 2 for each of the phases the steel is made of:

**Table 2.** The material properties for the A533 steel, from Desalos [26].

|  | Phase $\alpha$ | Phase $\gamma$ |
|---|---|---|
| Young's modulus (MPa) | 182,000 | 182,000 |
| Poisson ratio | 0.3 | 0.3 |
| Yield limit (MPa) | 950 | 145 |

## Constitutive equations of the Leblond et al.'s model

Transformation plasticity arises from two distinct mechanisms: the Greenwood and Johnson mechanism, where microscopic plastic strain results from volume incompatibilities between phases and is aligned by applied stress, and the Magee and Paxton mechanism (pertaining to martensitic transformation), where applied stress affects the orientation of emerging martensite plates. Experimental evidence supports this phenomenon by subjecting specimens to constant stress during formation. In typical scenarios involving small, uniaxial stress (such as in the x-direction), the resulting strain takes the form:

*Classical model.* The total strain tensor $\underline{\underline{\varepsilon}}^t$ is first defined, decomposing into three components: the elastic strain tensor $\underline{\underline{\varepsilon}}^e$, the thermal strain tensor $\underline{\underline{\varepsilon}}^{th}$, and the plastic strain tensor $\underline{\underline{\varepsilon}}^p$:

$$\underline{\underline{\varepsilon}}^t = \underline{\underline{\varepsilon}}^e + \underline{\underline{\varepsilon}}^{th} + \underline{\underline{\varepsilon}}^p. \tag{73}$$

The thermal deformation $\underline{\underline{\varepsilon}}^{th}$ encompasses the spherical component of the transformation deformation. The plastic deformation $\underline{\underline{\varepsilon}}^p$ includes the deviatoric part of the transformation deformation:

$$\begin{cases} \underline{\underline{\Sigma}} = \langle \underline{\underline{\sigma}} \rangle_V \\[2mm] \underline{\underline{d}}^t = \langle \underline{\underline{\varepsilon}}^t \rangle_V. \end{cases} \tag{74}$$

From this, at the macroscopic scale, emerges equation (75), which involves a decomposition of the total macroscopic deformation tensor $\underline{\underline{d}}^t$ into the contributions of elastic deformation $\underline{\underline{d}}^e$, thermo-metallurgical deformation $\underline{\underline{d}}^{thm}$, and plastic deformation $\underline{\underline{d}}^p$:

$$\underline{\underline{d}}^t = \underline{\underline{d}}^e + \underline{\underline{d}}^{thm} + \underline{\underline{d}}^p. \tag{75}$$

The following hypothesis is now introduced:

Hypothesis 1: The macroscopic flexibility tensor $\underline{\underline{M}}$ is assumed to be analogous to the microscopic flexibility tensor $\underline{\underline{m}}$, enabling the formulation of the following expressions:

$$\begin{cases} \underline{\underline{d}}^e = \langle \underline{\underline{\varepsilon}}^e \rangle_V = \underline{\underline{M}} : \underline{\underline{m}} \\[2mm] \underline{\underline{d}}^{thm} = \langle \underline{\underline{\varepsilon}}^{th} \rangle_V = (1-z)\underline{\underline{\varepsilon}}^{th}_M + z\underline{\underline{\varepsilon}}^{th}_D \\[2mm] \underline{\underline{d}}^p = \langle \underline{\underline{\varepsilon}}^p \rangle_V \end{cases} \tag{76}$$

The thermo-metallurgical deformation ($\underline{\underline{\varepsilon}}^{thm}$) is determined experimentally through free dilatometry testing. However, the plasticity deformation ($\underline{\underline{\varepsilon}}^p$) is not straightforward to ascertain; it involves the classical plasticity

$(\underline{\varepsilon}^{cp})$ and the transformation deformation $(\underline{\varepsilon}^{tp})$. It is worth noting that plastic deformation considers the volumetric variation of each phase and, consequently, the position of the boundary $(F)$ between the two phases. When differentiating $\underline{\varepsilon}^p$ with respect to time, the following formula arises:

$$\underline{\dot{\mathbf{d}}}^p = \frac{d}{dt}\left[\frac{1}{\mathrm{Vol}(V)}\int_V \underline{\varepsilon}^p\,dv\right] = (1-z)\langle\underline{\dot{\varepsilon}}_M^{th}\rangle_{V_M} + z\langle\underline{\dot{\varepsilon}}_D^p\rangle_{V_D} + \dot{z}\langle\Delta\underline{\varepsilon}_{M\to D}^p\rangle_{F(U_n)}, \tag{77}$$

where

$$\begin{cases} \langle\underline{\dot{\varepsilon}}_i^p\rangle_{V_i} & \text{Mean of } \underline{\dot{\varepsilon}}_i^p \text{ over the volume } V_i\,(i=M,D) \\[2mm] F & \text{tip of the transformation} \\[2mm] U_n & \text{normal to the front of advance of } F \end{cases} \tag{78}$$

and $\langle\Delta\underline{\varepsilon}_{M\to D}^p\rangle_{F(U_n)}$ is the average of the discontinuity surface of $\Delta\underline{\varepsilon}_{M\to D}^p$ under the transformation tip weighted by the velocity normal vector $U_n$:

$$\langle\Delta\underline{\varepsilon}_{M\to D}^p\rangle_{F(U_n)} = \frac{\displaystyle\int_F \Delta\underline{\varepsilon}_{M\to D}^p U_n\,dS}{\displaystyle\int_F U_n\,dS}. \tag{79}$$

The discontinuity of $\underline{\varepsilon}^p$ across the two phases arises from the fact that the deviatoric part of the transformation strain is introduced into plastic deformation, causing a deformation jump when passing through these two zones. By convention, $\dot{z} > 0$ as the boundary $F$ moves from the daughter phase $\alpha \equiv D$ to the parent phase $\gamma \equiv M$. The thermoplastic behavior leads to stating the classical plastic strain rate $\dot{\mathbf{d}}^{cp}$ as related to the temperature evolution $\dot{T}$ and the stress rate $\underline{\dot{\Sigma}}$:

$$\underline{\dot{\mathbf{d}}}^{cp} = \underline{\dot{\mathbf{d}}}_\Sigma^{cp} + \underline{\dot{\mathbf{d}}}_T^{cp}. \tag{80}$$

And for the plastic deformation rate of transformation $\underline{\dot{\mathbf{d}}}^{tp}$, it only occurs during the transformation, meaning that it depends on $\dot{z}$. Now, the plastic deformation rate $\underline{\dot{\mathbf{d}}}^p$ defined in equation (79) can be expressed entirely as a decomposition of $\underline{\dot{\varepsilon}}^p$ in terms proportional to $\underline{\dot{\Sigma}}$, $\dot{T}$, and $\dot{z}$.

In a typical problem of ordinary mechanics at the local scale, it arises:

$$\underline{\dot{\varepsilon}}^p = (\,)\underline{\dot{\Sigma}} + (\,)\dot{T} \tag{81}$$

without the term proportional to $z$ but since

$$\underline{\dot{\sigma}}^p = (\,)\underline{\dot{\Sigma}} + (\,)\dot{T} + (\,)\dot{z} \tag{82}$$

the expression for $\underline{\dot{\varepsilon}}^p$ follows:

$$\underline{\dot{\varepsilon}}^p = \left(\frac{\delta\underline{\dot{\varepsilon}}^p}{\delta\underline{\Sigma}}\right)\underline{\dot{\Sigma}} + \left(\frac{\delta\underline{\dot{\varepsilon}}^p}{\delta T}\right)\dot{T} + \left(\frac{\delta\underline{\dot{\varepsilon}}^p}{\delta z}\right)\dot{z}. \tag{83}$$

Using the equation below, taken from the volumes $V_M$ and $V_D$, equation (77) becomes:

$$
\begin{aligned}
\underline{\dot{\mathbf{d}}}^p =\ & \underbrace{\left\{ (1-z)\left\langle \frac{\delta \underline{\underline{\dot{\varepsilon}}}_M^p}{\delta \underline{\underline{\Sigma}}} \right\rangle_{V_M} + z\left\langle \frac{\delta \underline{\underline{\dot{\varepsilon}}}_D^p}{\delta \underline{\underline{\Sigma}}} \right\rangle_{V_D} \right\} \underline{\underline{\dot{\Sigma}}}}_{\underline{\underline{\dot{\mathbf{d}}}}_{\underline{\underline{\Sigma}}}^{cp}} \\[2mm]
& + \underbrace{\left\{ (1-z)\left\langle \frac{\delta \underline{\underline{\varepsilon}}_M^p}{\delta T} \right\rangle_{V_M} + z\left\langle \frac{\delta \underline{\underline{\dot{\varepsilon}}}^p}{\delta T} \right\rangle_{V_D} \right\} \dot{T}}_{\underline{\underline{\dot{\mathbf{d}}}}_T^{cp}} \\[2mm]
& + \overbrace{\left\{ \underbrace{(1-z)\left\langle \frac{\delta \underline{\underline{\varepsilon}}_M^p}{\delta z} \right\rangle_{V_M} + z\left\langle \frac{\delta \underline{\underline{\varepsilon}}_D^p}{\delta z} \right\rangle_{V_D}}_{\text{Greenwood and Johnson mechanism}} + \underbrace{\langle \Delta \underline{\underline{\varepsilon}}_{M\to D}^p \rangle_{F(U_n)}}_{\text{Magee and Paxton mechanism}} \right\} \dot{z}}^{\underline{\underline{\dot{\mathbf{d}}}}^{tp}} .
\end{aligned}
$$

In this way, in the previous equation, the terms averaged over the volume of the phases are due to the Greenwood and Johnson mechanism [29] (plastic volumetric accommodation), while the term integrated over the advancement front of the transformation is linked to the Magee and Paxton mechanism [7] (effect of the orientation of the transformation deformation).

In order to arrive at the explicit expression $(\underline{\underline{\dot{\mathbf{d}}}}^{tp} = \frac{2}{3}K\underline{\underline{\mathbf{S}}}\phi'(z)\dot{z})$ of Leblond [30], he first assumes that the transformations are diffusive and that only the Greenwood and Johnson mechanism [29] matters; this would have implied that

$$
\underline{\underline{\dot{\mathbf{d}}}}^{pt} = \left\{ \underbrace{(1-z)\left\langle \frac{\delta \underline{\underline{\varepsilon}}_M^p}{\delta z} \right\rangle_{V_M} + z\left\langle \frac{\delta \underline{\underline{\varepsilon}}_D^p}{\delta z} \right\rangle_{V_D}}_{} \right\} \dot{z} \tag{84}
$$

and the following hypotheses are made:

- **Hypothesis 1:** The macroscopic flexibility tensor **M** is assumed to be analogous to the microscopic flexibility tensor **m**.
- **Hypothesis 2:** For low applied efforts, the $\gamma$ phase is entirely plastic, but the $\alpha$ phase remains elastic. In other words, the plastic deformation rate of the parent phase (austenite) is much lower than that of the daughter phase (ferrite, martensite) and this implies that

$$
\underline{\underline{\dot{\mathbf{d}}}}^{pt} = (1-z)\left\langle \frac{\delta \underline{\underline{\varepsilon}}_M^p}{\delta z} \right\rangle_{V_M} \dot{z}. \tag{85}
$$

- **Hypothesis 3:** And obeying the von Mises criterion and the associated Prandtl-Reuss flow law:

$$
\underline{\underline{\dot{\mathbf{d}}}}^{pt} = \frac{3(1-z)}{2\sigma_Y^M} \left\langle \frac{\delta \varepsilon_M^{eq}}{\delta z} \underline{\underline{\mathbf{s}}}_M \right\rangle_{V_M} \dot{z}, \tag{86}
$$

with

$$
\begin{cases}
\sigma_Y^M & \text{elastic limit of the parent phase} \\[3mm]
\underline{\underline{\mathbf{s}}}_M & \text{microscopic deviatoric tensor} \\[3mm]
\varepsilon_M^{eq} & \text{equivalent strain.}
\end{cases} \tag{87}
$$

- **Hypothesis 4:** The correlation between $\dfrac{\delta\varepsilon_M^{eq}}{\delta z}$ and $\underline{\underline{s}}_M$ can be neglected. As a result,

$$\dot{\underline{\underline{d}}}^{pt} = \frac{3(1-z)}{2\sigma_Y^M}\left\langle\frac{\delta\varepsilon_M^{eq}}{\delta z}\right\rangle_{V_M}\underline{\underline{S}}_M\dot{z}, \tag{88}$$

where $\underline{\underline{S}}_M = \langle\underline{\underline{s}}_M\rangle_{V_M}$ is the average of the stress deviatoric part in phase $M$.

- **Hypothesis 5:** For small applied stresses, the average deviatoric stresses in phase $M$ are approximately equal to the average deviator of the overall stresses, $\underline{\underline{S}}_M = \underline{\underline{S}} = \langle\underline{\underline{s}}_M\rangle_V$; with this we have:

$$\dot{\underline{\underline{d}}}^{pt} = \frac{3(1-z)}{2\sigma_Y^M}\left\langle\frac{\delta\varepsilon_M^{eq}}{\delta z}\right\rangle_{V_M}\underline{\underline{S}}\dot{z}. \tag{89}$$

*Spherical growth model of LEBLOND for the GREENWOOD-JOHNSON mechanism.* For the effective calculation of the magnitude $\left\langle\dfrac{\delta\varepsilon_M^{eq}}{\delta z}\right\rangle_{V_M}$ (and no longer $\left\langle\dfrac{\delta\underline{\underline{\varepsilon}}_M^p}{\delta z}\right\rangle_{V_M}$ which averages to zero), Leblond proposes, in the case of low applied stresses (this calculation is actually done for $\underline{\underline{\Sigma}} = \underline{\underline{0}}$), that the ferritic structure (phase $\alpha \equiv D$) is a spherical inclusion that grows inside an austenitic sphere (phase $\gamma \equiv M$).

The main objective is to evaluate the quantity $\left\langle\dfrac{\delta\underline{\underline{\varepsilon}}_M^p}{\delta z}\right\rangle_{V_M}$ from expression (89), which represents the average increase in equivalent plastic deformation of the parent phase induced by a slight increase in the proportion of the daughter phase.

After a simplified micro-mechanical calculation, Leblond and coworkers finally determine the formula for the transformation strain rate as follows:

$$\dot{\underline{\underline{d}}}^{pt} = -3\frac{\Delta\varepsilon_{1\to2}^{th}}{\sigma_Y^M}\underline{\underline{S}}\,(\ln(z))\,\dot{z}. \tag{90}$$

And by identifying with equation ($d_{11}^{pt} = K\Sigma_{11}\phi(z)$), it follows that

$$\begin{cases} K = \dfrac{\Delta\varepsilon_{1\to2}^{th}}{\sigma_Y^M} \\[2mm] \phi(z) = z\,(1 - \ln(z)) \end{cases}. \tag{91}$$

Finally, Leblond et al. [11] complement this theoretical approach with finite element numerical calculations on a diffusional transformation in A508 steel, in order to:

- Check the validity of the hypotheses adopted during the definition of the theoretical model;
- Look for a flow rule expression whose validity domain is broader than that allowed by the theoretical expression (90).

Thus, the model by Leblond et al. [11] was developed in various forms to predict different types of behaviors (perfect plasticity, isotropic hardening, or kinematic hardening) and applied loading levels. These laws are listed in three sections below:

*Leblond et al. model without strain hardening*

- At lower stresses:

$$\dot{\underline{\underline{d}}}^{pt} = \begin{cases} \underline{\underline{0}} & \text{if } z \leq 0.003 \\[3mm] -3\dfrac{\Delta\varepsilon_{1\to2}^{th}}{\sigma_Y^M}h\left(\dfrac{\Sigma_{eq}}{\Sigma_Y}\right)\underline{\underline{S}}\,(\ln(z))\,\dot{z} & \text{if } z > 0.003, \end{cases} \tag{92}$$

where

$$h\left(\frac{\Sigma_{eq}}{\Sigma_Y}\right) = \begin{cases} 1 & \text{if } \frac{\Sigma_{eq}}{\Sigma_Y} \leq \frac{1}{2} \\[2ex] 1 + 3.5\left(\frac{\Sigma_{eq}}{\Sigma_Y} - \frac{1}{2}\right) & \text{if } \frac{\Sigma_{eq}}{\Sigma_Y} > \frac{1}{2}. \end{cases} \tag{93}$$

- At higher stresses:

$$\underline{\dot{\underline{d}}}^p = \dot{\Lambda}\underline{\underline{S}}. \tag{94}$$

*Leblond et al. model with isotropic strain hardening*

- At lower stresses:

$$\underline{\dot{\underline{d}}}^{pt} = \begin{cases} \mathbf{0} & \text{if } z \leq 0.003 \\[2ex] -3\dfrac{\Delta\varepsilon^{th}_{1\to2}}{\sigma^M_Y(E^{eff}_M)}h\left(\dfrac{\Sigma_{eq}}{\Sigma_Y}\right)\underline{\underline{S}}\,(\ln(z))\,\dot{z} & \text{if } z > 0.003, \end{cases} \tag{95}$$

where

$$h\left(\frac{\Sigma_{eq}}{\Sigma_Y}\right) = \begin{cases} 1 & \text{if } \frac{\Sigma_{eq}}{\Sigma_Y} \leq \frac{1}{2} \\[2ex] 1 + 3.5\left(\frac{\Sigma_{eq}}{\Sigma_Y} - \frac{1}{2}\right) & \text{if } \frac{\Sigma_{eq}}{\Sigma_Y} > \frac{1}{2}, \end{cases} \tag{96}$$

$$E^{eff}_M = \begin{cases} -2\dfrac{\Delta\varepsilon^{th}_{1\to2}}{1-z}h\left(\dfrac{\Sigma_{eq}}{\Sigma_Y}\right)(\ln(z))\,\dot{z} + \dfrac{g(z)}{E}\dot{\Sigma}_{eq} & \text{if } z > 0.003 \\[3ex] -2\dfrac{\Delta\varepsilon^{th}_{1\to2}}{1-z}h\left(\dfrac{\Sigma_{eq}}{\sigma^M_Y}\right)(\ln(z))\,\dot{z} + \dfrac{g(z)}{E}\dot{\Sigma}_{eq} + \dfrac{2(\alpha_M - \alpha_D)}{1-z}z\ln(z)\dot{T} & \text{if } z \leq 0.003, \end{cases}$$

- At higher stresses:

$$\underline{\dot{\underline{d}}}^p = \frac{3}{2}\frac{\dot{E}_{eq}}{\dot{\Sigma}_{eq}}\underline{\underline{S}}. \tag{97}$$

*Leblond et al. model with kinematic strain hardening*

- At lower stresses:

$$\underline{\dot{\underline{d}}}^{tp} = \begin{cases} \underline{\underline{\mathbf{0}}} & \text{if } z \leq 0.003 \\[2ex] -3\dfrac{\Delta\varepsilon^{th}_{1\to2}}{\sigma^M_Y}h\left(\dfrac{\Sigma_{eq}}{\Sigma_Y}\right)\left(\underline{\underline{S}} - \underline{\underline{A}}_{\mathbf{M}}\right)(\ln(z))\,\dot{z} & \text{if } z > 0.003, \end{cases} \tag{98}$$

where

$$h\left(\frac{\Sigma_{eq}}{\Sigma_Y}\right) = \begin{cases} 1 & \text{if } \frac{\Sigma_{eq}}{\Sigma_Y} \leq \frac{1}{2} \\[2ex] 1 + 3.5\left(\frac{\Sigma_{eq}}{\Sigma_Y} - \frac{1}{2}\right) & \text{if } \frac{\Sigma_{eq}}{\Sigma_Y} > \frac{1}{2}. \end{cases} \tag{99}$$

- At higher stresses:

$$\underline{\dot{\underline{d}}}^{tp} = \frac{3}{2}\frac{\dot{d}_{eq}}{\dot{\Sigma}_{eq}}\left(\underline{\underline{S}} - \underline{\underline{A}}\right). \tag{100}$$

*Naming convention for the parameters utilized in Leblond et al.'s model.*

- $\Sigma_{eq}$: equivalent stress
- $\Sigma_Y$: the homogenized macroscopic yield strength
- $\sigma_Y^M$: the yield strength of the parent phase
- $\Delta\varepsilon_{1\to2}^{th}$: the thermal deformation difference between the two phases
- $\mathbf{S}$: deviatoric part of the stress tensor $\Sigma$
- $z$: ratio of the daughter phase
- $E_M^{eff}$: cumulative plastic deformation in the parent phase
- $E_D^{eff}$: cumulative plastic deformation in the daughter phase
- $g(z)$: function related to the created phase
- $E$: Young's modulus
- $\underline{\underline{\mathbf{A}}}$: homogenized kinematic hardening variable
- $\underline{\underline{\mathbf{A}}}_M$: kinematic hardening variable linked to the parent phase
- $\alpha_M$: thermal expansion coefficient of the mother phase
- $\alpha_D$: thermal expansion coefficient of the daughter phase
- $T$: the temperature
- $\underline{\underline{\dot{\mathbf{d}}}}^p$: rate of plastic deformation
- $\dot{d}_{eq}$: equivalent plastic strain rate
- $h\left(\frac{\Sigma_{eq}}{\Sigma_Y}\right)$: function representing the non-linearity of plastic deformation transformation